Published in final edited form as:

Nanoscale. 2020 May 07; 12(17): 9306–9326. doi:10.1039/c9nr10963c.

Functional Nanoarrays for Investigating Stem Cell Fate and Function

Jin-Ho Lee[†,a,b,c], **Jeffrey Luo**[†,a], **Hye Kyu Choi**[b], **Sy-Tsong Dean Chueng**[a], **Ki-Bum Lee**[a], **Jeong-Woo Choi**[b]

[a.]Department of Chemistry and Chemical Biology, Rutgers University, Piscataway, NJ 08854, USA.

[b.]Department of Chemical and Biomolecular Engineering, Sogang University, Seoul, 121-742, Korea.

[c.]School of Biomedical Convergence Engineering, Pusan National University, Yangsan 50612, Korea

Abstract

Stem cells offers excellent potential in the field of tissue engineering and regenerative medicine based on their excellent capability to not only self-renew but also differentiate into a specialized cell type of interest. However, the lack of a non-destructive monitoring system renders it challenging to identify and characterize differentiated cells before their transplantation without compromising cell viability. Thus, the development of a non-destructive monitoring method for analyzing cell function is highly desired and can significantly benefit stem cell-based therapies. Recently, nanomaterial-based scaffolds (e.g., nanoarray) have made possible considerable advances in controlling the differentiation of stem cells and characterization ofing the differentiation status sensitively in realtime. This review provides a selective overview of the recent progress in synthesis methods of nanoarray as well as its applications for controlling stem cell fate and monitoring live cell functions electrochemically. We believe the topics discussed in this review can provide a brief and concise guideline in the development of novel nanoarrays and promote the interest in live cell study applications. The A method which that can not only control but also monitor stem cell fate and function will be a promising technology that can accelerate stem cell therapies.

Graphical Abstract

Overview of the recent progress of nanoarray synthesis and applications for controlling stem cell fate and monitoring live cell functions.

[†]Equally contributed.

Electronic Supplementary Information (ESI) available: [details of any supplementary information available should be included here]. See DOI: 10.1039/x0xx00000x

Conflicts of interest

The authors do not have any conflicts of interest to declare.

Stem cell therapy is emerging as the next major development in regenerative medicine for functional recovery of tissues and organs damaged by aging, disease, or injuries.[1–3] Accordingly, an improved understanding of stem cells and control of stem cell fate is likely to benefit treatments for devastating diseases and injuries.[3–5] However, a significant drawback in current stem cell therapy is the limited control of stem cell fate, which leads to low efficiency in generating maturely differentiated cells that can replace the damaged original tissues and organs.[6–8] Addressing the current challenges, researchers have invested in the development of biomaterials that mimic the chemical and mechanical properties of native environments in order to manipulate and control stem cell fate and function in a more precise and defined manner.[9–12] However, despite the numerous breakthroughs in our understanding of the biological cues that drive stem cell behavior, mimicking native environments remains difficult.

Typically, during stem cell differentiation, cells interact with the surrounding extracellular matrix (ECM), and a variety of intracellular events are influenced by its definable chemical and mechanical properties.[9, 10] Therefore, mechano-structural properties of the ECM play a significant role in regulating stem cell behaviors. Recently, considerable advancement in nanoarray research has lead to the development of sophisticated techniques and materials that can exploit the properties of ECM scaffolds to control cell behavior and repair tissues.[11, 12] While innumerable cell processes differ between different cell types, certain key pathways such as integrin-binding, receptor clustering, and other mechano-transduction cascades remain relatively conserved.[13] For example, integrin signaling is intimately connected to numerous pathways. Osteogenesis (formation of osteoblasts and bone) has been correlated with stiff substrates, while adipogenesis (formation of adipocytes and fat) has been correlated with soft substrates.[14] Soft substrates (e.g., an adipose microenvironment) promote an increase in active β1 integrin, which in turn causes the internalization of BMPR (BMP receptor).[15, 16] This results in decreased BMP/Smad activity, along with decreased osteogenesis. Interestingly, knockdown of β1 integrins has the paradoxical effect of decreasing osteogenesis.[17] On the other hand, activation of α2 due to cell seeding on stiff substrates leads to an increase in osteogenesis.[16, 18] The role of α2 in osteogenesis is further supported by prior reports whereby knockdown of α2 was found to decrease YAP/TAZ translational activity, which decreases osteoblast formation.[19, 20] The at-times contradicting and constantly evolving understanding of substrate stiffness and stem

cell differentiation underlines the interplay and complexity associated with mechano-transduction pathways. To this end, mechano-transduction pathways between nanotopography and cell interaction will be thoroughly discussed in this review in order to examine the interaction between substrate topography and cell behavior and enable designing of nanoarrays for pathway-specific stem cell differentiation. A discussion regarding basic biological mechanisms will help lay the foundation for understanding the factors that influence how and why stem cells respond to substrates, including surface chemistry and substrate topography.[21–25]

One of the current hurdles for most cell characterization methods, such as qPCR and immunostaining, is the requirement for a destructive step, which hinders the safety and effectiveness of stem cell-based therapy.[26, 27] To this end, nondestructive characterization techniques have gained interest for monitoring stem cell behaviors while maintaining a healthy cell population for transplantation.[28–31] Specifically, functional nanoarrays have gained tremendous attention due to expanding efforts to integrate the concepts of nanochemistry and topography into clinically useful applications.[28, 29] While biological studies continuously elucidate the role of substrate topography in influencing clinically advantageous stem cell behavior (e.g., enhanced differentiation), nanochemistry enables the development of more accurate and sensitive detection methods (e.g., signal enhancement). Therefore, there is a significant interest in developing devices that leverage these unique advantages into an integrated nanoarray capable of non-destructively monitoring stem cells as they differentiate, through rationally designed topographical cues.

Although many reviews address stem cell therapy for use in regenerative medicine,[8, 32, 33] the tremendous amount of recent activity on nanoarray for stem cell therapy and a new, live cell-based monitoring approach warrant a thorough review at this time. This review will provide an extensive analysis of the current state-of-the-art developments in the field. More specifically, emphasis will be placed on (i) recent advances in the synthesis methods of nanoarray, (ii) design and characterization of advanced nanoarray that provides environmental insoluble cues (nanotopography effect) for stem cell therapy and (iii) its application to non-destructive characterization methods [Figure 1]. We envision that this article will inspire interest from various disciplines and highlight an important field wherein great strides are being made towards the use of advanced nanoarray systems in the clinical application of stem cell therapy for regenerative medicine.

2. Nanoarray Fabrication Methods

Functional nanoarray has considerably advanced the field of stem cell-based therapy by providing both topographical effects on stem cell behaviors and improving the sensitivity of analytical monitoring systems.[28, 29] Accordingly, different synthesis methods have profound effects on the morphology, compositions, and properties of the generated functional nanoarray. Due to the ubiquity and unparalleled pattern control offered by various lithography techniques, we will focus on the most well-defined techniques, including hydrothermal deposition, chemical/physical vapor deposition, electrical/electrochemical deposition, and template-assisted nanopattern array generation.

2.1 Hydrothermal Deposition Methods

The conventional hydrothermal deposition method, based on wet chemistry, typically involves hydrolysis and precipitation reactions from a chemical-based aqueous solution to generate nanostructures such as nanoarrays on various shaped substrates.[34–36] In general, this facile and cost-effective hydrothermal deposition method has been known to be highly efficient in the generation of various shapes and kinds of metal oxide nanostructures.[37, 38] Typically the geometry and distribution of nanoarrays can be varied by altering experimental parameters, including pH value, temperature, reaction time, and chemical concentration, including that of the precursor. For example, Gao et al. successfully synthesized well-oriented double-layered lanthanum-doped SnO_2 nanoarrays by a substrate-free hydrothermal deposition method.[39] By adjusting the lanthanum chloride ($LaCl_3{\cdot}6H_2O$) concentration, a controlled morphology and phase structure can be obtained. On occasion, the deposition of seeds as a prior step could facilitate the nucleation and growth of nanoarrays on substrates. To explore this effect, Cook et al. hydrothermally synthesized ZnO nanowire on seedless and ZnO-seeded graphene and investigated the effects on the structural geometries.[40] On the other hand, to scale-up this hydrothermal deposition-based process, Wang et al. implemented a continuous flow technique to synthesize uniform ZnO nanorod arrays on 3-D honeycomb substrates.[41] The growth of ZnO nanorod arrays is similar to typical hydrothermal processes. The the ZnO seed layer was deposit on wall surfaces of multi-channeled monolithic substrates and followed by hydrothermal growth of large-scale ZnO nanorod arrays. However, comparably, significantly improved uniformity and alignment were obtained through integration with a continuous flow technique. The continuous flow-assisted mass transport in a confined space significantly enhanced nucleation and growth rate of nanostructure on the substrates. Overall, the hydrothermal deposition-based method has proved to be highly efficient, facile, and cost-effective for the growth of various nanostructures on a large scale.

2.2 Chemical/Physical Vapor Deposition Methods

Chemical/physical vapor deposition (CVD/PVD) is a vapor phase deposition process wherein the desired material is produced by surface exposure and a reaction of gaseous precursors on the surface of the substrate.[42–44] It has been widely employed to fabricate nanoarrays with high crystallinity and fewer defects. These processes typically require the precise control of various experimental parameters such as pressure, temperature, and precursor concentration. Generally, to obtain high-crystallinity nanomaterials, high pressure, temperature, and a conductive film layer are required as a catalysts. For example, high crystallinity of the ZnO nanowires can be generated on Si substrate at high temperatures with a coated layer of gold film as a catalyst;[45] however, the use of metal catalysts tend to contaminate the final products, and the catalyst droplets at the growing end of the nanowires can affect the properties of the final nanostructures. Therefore, the direct growth of ZnO nanowires on a common dielectric substrate, such as SiO_2, with the CVD method is of great interest. Xu et al. have grown single-crystalline ZnO nanowire arrays directly on a SiO_2 substrate on a large scale using the CVD approach.[46] As prepared, Si substrate was etched to carve out spikes and valleys. After formation, the ZnO nanoclusters act as nucleation sites, which result in the subsequent growth of ZnO nanowires. Uniform size and morphological distribution of ZnO nanowires were achieved with a preferential growth direction along

[001]. Similarly, Chen and coworkers have developed a quasi-aligned single-crystalline 3C-SiC nanowire (3C-SiCNW) array with tailored shapes using nitrogen-doping (N-doping) on a flexible carbon fabric. This result has shown the possibility of the utilization of nanoarray fabrication methods to develop flexible electronics that can be integrated into the textiles or used in portable electronics.[47] As can be seen, this gas-phase technique offers the benefit of higher purity deposition on various substrates; however, high vacuums may still be required for non-volatile substrates, and hazardous by-products such as CO, H_2, and HF can be generated in the process, which should be addressed.

2.3 Electro/Electrochemical Deposition Methods

Electro/electrochemical deposition is a widely adopted method for the development of nanoarrays. Electro/electrochemical deposition involves reduction and oxidation (redox) processes, which result in the formation of insoluble precipitates on the surface of the electrode.[48–51] The final composition and structural morphology can be easily altered through modulation of several experimental parameters such as solution composition, potential voltage, current density, deposition time, or electrode substrate. Wang et al. demonstrated electrochemical deposition of thorn-like Ni@TiC nanowire arrays and flake-like Co@TiC nanoarrays electrodes, which are fabricated by the electrodeposition of Ni and Co catalysts on TiC nanowire arrays.[52] Instead of applying constant potential, Gioia et al. used pulse potential and generated palladium species on multi-walled carbon nanotubes dispersed in a Nafion membrane.[53] A pulsed electrodeposition method is a deposition process wherein an applied potential or current density alternates between two or more potential values. Thus, nucleation and crystallization can be controlled by the potential pulse amplitude and duration, which results in excellent mono-sized dispersion. Since these electro/electrochemical methods can only deposit the material of interests onto a conductive surface from a solution containing the corresponding precursor salts, its application is limited to the production of nanostructures on semiconductor and nonconducting substrates.

2.4 Template-Assisted Methods

The template-assisted method is considered to be an ideal synthesis technique for the design and development of a highly precise pattern array. In general, the template-assisted approach produces a highly ordered nanostructure and allows for control of both size and structure periodicity in a precise manner.[54–58] Anodized aluminum oxide (AAO) is one of the most widely utilized materials owing to ease of fabrication, highly ordered pore structure with a controllable pore size, and the amenable ability to be removed with basic solutions. By adjusting anodization time, potential, and the electrolyte solution composition, nanopores with different lengths and diameters can be generated. Subsequently, on the as-synthesized AAO template, a thin layer of electrically conductive material, such as silver, can be pre-coated on one side of the AAO template to serve as the current collector.[30] Then the electroactive materials can electro/electrochemically deposited into the nanopores to form highly ordered nanoarrays.[59]

However, AAO template-based nanoarray development has been highly restricted to smooth and inert surfaces. To address this challenge, Robatjazi et al. presented a new strategy for the fabrication of nanostructures with sub-100 nm diameters on both smooth and rough

substrates by preparing a free-standing through-hole ultrathin alumina membrane (UTAMs).[60] UTAMs with highly regular arrays of pores were prepared via two-step anodization of high-purity aluminum foil. To obtain UTAM containing pores on both sides without breaking of the structure, a thin layer of polystyrene was coated on the UTAMs, and the aluminum base layer was thoroughly detached. After the removal of the polystyrene layer in chloroform, a free-standing through-hole UTAM floating on water was successfully obtained. By using the obtained UTAM as a template, a highly ordered nanoarray was able to be developed on both smooth and rough substrates [Figure 2].

Due to difficulties in the development of heterogeneous nanostructure assembly on a large scale, the majority of recent work has focused on developing a single-component nanoarray. In this regard, a new concept for design and fabrication of binary heterogeneous architecture arrays using a binary pore AAO template has been proposed by Wen and coworkers.[61, 62] By employing an over-etching process to partially expose four edges of one set of nano components in a binary-pore template and selective deposition, a densely packed, heterogeneous nanostructure array was successfully created. The controlled size and shape, as well as inter-pore spacing, could be used to generate various nanostructure arrays with the assistance of binary-pore templates and deposition. In a different manner, Zhao et al. created multi-layer nanoarrays sandwiched by anodized aluminum oxide membranes.[55] Instead of sacrificing the AAO template, it was preserved as a part of the nanostructure to support the second and third layers of multilayer metal arrays.

3. Effects of substrate nanotopography on cellular behaviors

To fully exploit the clinical potential of cell-based therapies, it is advantageous to characterize and utilize all facets of cell behaviors to promote key beneficial processes such as stem cell proliferation and differentiation. Integrins are well-known cell membrane receptors that play a pivotal role in interpreting physical extracellular cues during numerous cell processes. Each of the 24 known final protein assemblies consists of one α subunit (of which there are 18 types), paired with one β subunit (of which there are 8 types) (heterodimeric molecules).[21] These final pairings, in turn, respond to different stimuli (e.g., binding to ECM proteins versus other cells expressing membrane surface adhesion molecules) and have differing effects on cell behaviors. For example, a bone regenerating device may be used to encourage osteogenesis (formation of bone and bone-building cells such as osteoblasts). In this situation, it would be beneficial to stimulate integrins containing the α2 subunit (involved in modulation of osteogenesis) and hinder activity associated with β3 integrins (involved in modulation of myogenesis) to ensure the occurrence of the intended cell behaviors.[63]

While integrin signals are involved in a multitude of other signaling pathways, one particularly important and interesting downstream target is YAP/TAZ. Activation of YAP/TAZ via stiff surfaces for prolonged periods appears to activate a long-term “mechanical memory,” wherein constitutive activation of YAP remains even after cells are placed on a softer surface.[64] Thus, integrin signaling during prolonged cell culture (typically done on polystyrene flasks) may carry important implications for future use in applications such as regenerative therapies.

3.1 Synergistic Strategies for Modulating Cell Behaviors

While proper substrate design plays a pivotal role in manipulating cell activity, it is very common to integrate other elements into cell culture scaffolds to ensure greater control over desired behaviors. These elements may range from soluble factors in the culture media to external mechanical forces.[65–70]

Numerous small molecules and growth factors can be incorporated into cell substrates for sustained release during culture. For example, nanofibers can be loaded with stem cell differentiation factors to enable greater control over cell fate. One simple example is the incorporation of TGF-β1 into chitosan nanoparticles, which were then incorporated into aligned poly-caprolactone (PCL) and poly-L-lactic acid (PLLA) nanofibers.[67] The nanotopographical cues from the PCL-PLLA nanofibers induced significantly higher expression of smooth muscle markers calponin 1 and SM22α from seeded MSCs, as compared to a tissue culture plastic control. Notably, the inclusion of TGF-β1 into the nanofiber, as opposed to supplementation in the cell culture media, enables higher expression of smooth muscle α-actin. Numerous other payloads in other materials can be found elsewhere in literature by groups that seek to achieve a similar goal: incorporation of growth factors into their substrates. This concept of incorporating soluble cues (e.g., TGF-β1 for myogenesis) into substrates with nanotopography (e.g., aligned nanofibers for myogenesis and cell alignment) can enable continued control over cell behaviors after transplantation, since further *in vivo* manipulation can be difficult.

Another widely studied cell control mechanism is the modulation of cell-cell interactions, primarily by changing cell density. For example, chondrocytes and optimal chondrogenesis from MSCs require high densities ($0.5–1 \times 10^7$ cells/cm^3), leading to efforts to obtain enough cells to adequately enable chondrogenesis for large transplantation-scale scaffolds.[65, 66] Li et al. alternatively simulated cell-cell interactions by incorporation of N-cadherin mimetic peptides into fibrillar hydrogels to encourage chondrogenesis.[68] The authors appended an N-cadherin sequence onto a self-assembling peptide to incorporate the N-cadherin domain onto the fibrillar hydrogel, with minimal effects on the mechanical properties of the substrate. qPCR and Western blotting showed significant inhibition of Wnt pathway signaling, leading to increased chondrogenic protein expression[68]. This effect was short-lived, as most Wnt signaling and chondrogenic protein expression normalized between the N-cadherin-mimicking hydrogels and controls by day 14. Interestingly, N-cadherin-mimicking hydrogel glycosaminoglycan content (an integral feature of cartilage for maintenance of viscoelastic properties) remained elevated, as compared to controls even after day 14. This approach of simulating cell-cell interactions at lower cell densities can potentially serve to both enhance chondrogenesis and reduce time and material costs associated with obtaining the prerequisite number of cells before scaffold seeding.

Another approach that is similar to growth factor incorporation is surface immobilization. Whereas growth factor incorporation may not necessarily lead to a particular spatial arrangement for the payload, surface immobilization implies that the payload is presented on the substrate surface, where it can most readily interact with seeded cells. In one example, myogenesis was enhanced by using 3,4-dihydroxyphenylalanine (L-DOPA) to capture sphingosine-1-phosphate (S1P) on nanolithography-patterned polyurethane acrylate (PUA).

[69] The presence of S1P induces greater myogenesis of seeded C2C12 myoblasts. For substrates that undergo harsh processing conditions, which may denature or deactivate sensitive payloads, or are not biodegradable (e.g., encapsulated payloads unable to reach target cells), surface immobilization may be employed to ensure cells encounter the payload.

Carson et al. used a nanoarray with differing line dimensions to examine sarcomere development in cardiomyocytes.[70] The base substrate, PUA, is non-permissive for induced pluripotent stem cells (iPSC), so RGD domains were chemically grafted to enable cell adherence to the substrate. After a cardiomyocyte differentiation and maturation period, cells cultured on line patterns between 750–1000 nm showed significantly longer sarcomeres than cells cultured on a flat surface. While much work is still needed to elaborate on such mechanistic studies, they provide a framework for future efforts that aim to optimize a specific aspect of cell behavior (e.g., nanofiber substrates which promote cardiomyocyte maturation).

3.2.1 Enhanced, Lineage-specific Differentiation of Mesenchymal Stem Cells using Nanoarray—Interestingly, substrate stiffness can have significant implications on signaling pathways traditionally associated with soluble cues. For example, chondrogenesis is known to be suppressed when NK-κB is activated by peptides such as IL-1β and TNF-α. T. Jiang et al. developed PCL-polytetrahydrofuran (PCL-PTHF) nanofibers coated with collagen type 1 to mimic Young's modulus of cartilage.[71] The inclusion of collagen helped suppress the NK-κB pathway and promote expression of cartilage-specific genes, as compared to nanofibers without collagen. To determine the connection between collagen coating and enhanced chondrogenesis, the authors functionalized atomic force microscope (AFM) cantilevers with integrin subunit β1, which binds with collagen type 1. Cells cultured on collagen-functionalized nanofibers responded to the β1-AFM cantilevers similarly to native chondrocytes, while cells on glass or nonfunctionalized nanofibers responded similarly to MSCs. This difference was ablated by treating cells with PF-573228, which inhibits focal adhesions. While further experiments will be needed to solidify the role of integrin β1 signaling in the NK-κB pathway, pure topography-based approaches to stem cell differentiation can be advantageous, as they circumvent several problems associated with soluble cues, such as protein degradation and release kinetics.

Many load-bearing tissues (i.e., many MSC differentiation lineages) feature specific spatial arrangements and zonal organizations which assist with *in vivo* function. The design and characterization of substrates that can recapitulate these higher-order architectures from a single cell type can be of clinical value. One group examined nano-grates and nano-pillar topographies on several different materials [PCL, polylactide (PLA), and polyglycolide (PGA) in order of increasing compressive modulus] as a means of generating different zones reminiscent of articular cartilage.[72] Chondroitin sulfate was included as a surface coating to modulate the polyester surfaces for increased cell adhesion and chondro-inductiveness.[72] When stress fibers were analyzed by staining, stiffer substrates were found to induce significantly more intense and longer stress fibers than softer substrates.[72] Additionally, nano-pillar substrates resulted in less intense and shorter stress fibers than nano-grates, potentially due to differences in curvature.[72, 75] Cells seeded onto stiffer substrates preferentially expressed genes related to deeper cartilage zones: stiff nano-pillars induced

expression of ECM proteins common to osteochondral cartilage, while soft and intermediate nano-pillars induced gene expression reminiscent of middle/deep zones. Cells on soft and intermediate nano-gratings expressed proteins found in superficial cartilage.[72] This substrate stiffness-cartilage zone correlation mirrors natural cartilaginous tissue where deeper cartilage zones (superficial, middle/deep, osteochondral transition) are associated with the greatest resistance to compressive forces.[76] Unexpectedly, stiff nano-grates (longest stress fiber lengths) seemed to induce noncartilaginous tissue.[72] Given difficulties in inducing single stem-cell precursors to give rise to multiple controlled cell phenotypes via soluble factors (due to shared exposure to the same culture media), rationally designed substrates with graded substrate characteristics are an attractive alternative for the regeneration of tissues with heterogenous spatial arrangements.

To characterize MSC response to both micro- and nano-scale topography, G. Abagnale et al. utilized two different technologies to generate nano-grating of varying dimensions on polyimide chips.[63] Combinatorial micro-scale patterns were generated via reactive ion etching, while nano-scale patterns were generated via multi-beam interference. On the micro-patterned substrate, MSCs were more apt to differentiate into adipocytes when cultured on wider (15 μm) ridges, whereas smaller (2 μm) ridges were most conducive to osteogenesis. Interestingly, staining for vinculin revealed an absence of mature focal adhesions on substrates with smaller micro-ridges. When cultured on substrates monotonically patterned with 450 nm ridges and 200 nm grooves, both adipogenesis and osteogenesis were improved, as compared to a flat control. Despite the known role of YAP/TAZ in adipogenesis/osteogenesis and processes related to mechanotransduction, no difference in YAP cytoplasmic/nuclear localization was observed when comparing nano-grating to flat polyimide substrates. Both micro- and nano-scale patterns enabled cell alignment in parallel with the ridges. This paper provides an interesting distinction where micro-scale topography has vastly different effects (inducing distinct lineage preference) from nano-scale topography (generally increased differentiation efficiency) in a way that complements each other to enhance the final desired cell behavior (e.g. efficient generation of functional osteoblasts).

C. Zhao et al. tested the combination of micro- and nano-scale patterns on the same substrate for MSC osteogenesis.[73] In contrast with the other osteogenesis papers reported here, the authors opted to functionalize the substrate with hydroxyapatite (HA), which is a bioceramic widely used for its osteoinductive and osteoconductive properties.[73] Here, the authors developed a technique to compress HA microparticles along a micropattern and allowed HA nanorods to grow under a hydrothermal reaction. Substrates with micro-patterns and nano-rods, especially when combined, resulted in higher cell spreading, proliferation, and alkaline phosphatase (ALP) activity than the flat control. Combined micro-patterns and nano-rods resulted in elevated or comparable expression for key osteogenic genes BMP2, Runx2, ALP, and collagen type 1, as compared to the topographical features alone; all topographical features resulted in greater expression compared to the flat control. The described micro-patterns resulted in elevated α5, αv, and β1 expression, while the nano-rods only upregulated αv expression. Examination of specific BMP2 signaling receptors showed that micro-patterns, alone or combined, resulted in increased BMPR1A and BMPR1B, while nano-rods increased BMPR2 expression, indicating potentially different mechanisms at play

for different topography dimensions. Unexpectedly, nano-rods alone resulted in the highest osteocalcin expression. This suggests that different topography-length scales may be responsible for activation of different osteogenic pathways, and simultaneous activation of these pathways can result in greater osteogenic efficiency.

Rather than patterning substrates to generate regularly ordered topography, one group of researchers instead used reactive ion etching to create random, heterogeneous “nanorough” (root mean square roughness R_q = 1 for flat surfaces to R_q = 200 for roughest surface) surfaces for MSC osteogenesis [Figure 3].[74] Substrates with the highest roughness had the lowest proliferation, even in growth media. Conversely, MSC cultured on the roughest surface exhibited the greatest extent of osteogenesis (measured by ALP, osteopontin, osteocalcin, Runx2, and alizarin red activity) while showing no difference when directed towards adipogenesis. MSC on flat surfaces displayed larger, sparser focal adhesions that were evenly distributed along the cell area, whereas nanorough surfaces resulted in greater quantities of smaller focal adhesions primarily found on the cell periphery. Actin-myosin/stress fiber organization on nanorough substrates was described as intense and chaotic before aggregation, as compared to initial alignment when cultured on smooth surfaces. This stress fiber arrangement translated to MSC on nanorough surfaces exhibiting greater stiffness than cells on smooth surfaces. One interesting aspect of this research was the effort to determine whether nanorough substrates can replace canonical osteogenic small molecules. Here, the authors investigated dexamethasone, ascorbic acid, and β-glycerophosphate. Osteogenic differentiation media without dexamethasone was found to perform on par with complete differentiation media when cells were cultured on nanorough substrates, indicating that nanoroughness on these substrates can replace the biochemical signaling derived from dexamethasone. Interestingly, qPCR results indicate that ALP, Runx2, and osteopontin expression were upregulated for MSC cultured on nanorough substrates and in the absence of dexamethasone, as compared to complete media. Immunostaining for nuclear/cytoplasmic YAP showed that nanorough substrates were biased for YAP accumulation in the nucleus, which provides a probable mechanism for increased osteogenesis. Treatment with FAK inhibitor, Y-27632 (reduces stress fibers contractility), and cytoplasmin D (reduces actin polymerization) reduced nuclear YAP localization and ALP activity while lysophosphatidic acid, which increases stress fiber formation, had the reverse effect. Altogether, this paper supports the idea that differentiation factors thought to act via biochemical pathways may be replaced or supplanted by topographical cues.

3.2.2 Nanoarray-Guided Mature, Functional Neural Stem Cell Differentiation

—Like MSC, neural stem cells (NSC) respond to substrate stiffness. Adult rat-derived NSC cultured in the same mixed differentiation media (1% FBS, 2 mM glutamate, Neurobasal™ media) will undergo separate differentiation lineages when seeded on substrates with differing stiffness.[77] Due to the low Young’s modulus of native brain tissue, one group used chitosan methacrylamide to generate hydrogels at a physiologically relevant stiffness. Proliferation was maximized on hydrogels with Young’s modulus around 3.5 kPa and halted on hydrogels greater than 10 kPa. Additionally, both neuronal and astrocytic differentiation was most prominent when Young’s modulus was less than 1 kPa. For oligodendrogenesis, the authors suggested a biphasic mechanism where a greater number of NSC become

oligodendrocytes on stiffer substrates (e.g., 7 kPa) but reached maximum myelination and maturity on soft <1 kPa substrates. The authors suggest the presence of mature axons and myelination are intertwined, which would severely hinder oligodendrocyte development on stiffer substrates as neuronal development is shown to be most optimal at <1 kPa. Shah et al. expanded upon this concept further by generating PCL nanofibers (200–300 nm) to encourage NSC to adopt an oligodendrocyte fate by mimicking the presence of neuronal axons.[78] The authors noted that nanofibers, especially when coated with graphene oxide, augmented expression of key myelination-related genes. These two studies provide an excellent rationale for consideration of substrate stiffness and topography when dealing with neural cell lines.

Much of the work done to determine the role of substrates on NSC differentiation has mirrored work on MSCs. Factors such as stress fibers, contractility, and pharmacological agents for influencing these processes have been applied to NSC. For example, embryonic stem cells (ESC) induced into neural differentiation exhibit accelerated and aligned stress fiber formation when cultured on nano-grating patterns, as opposed to flat surfaces.[79] Adding blebbistatin (non-muscle myosin 2 inhibitor) or ML-7 (myosin light chain kinase inhibitor) caused decreases in stress fiber formation and MAP2 (mature neuron marker) expression. A qPCR array for 48 genes related to neurogenesis revealed that 14 genes were upregulated when cells were cultured on nano-grates. Similar to MAP2 staining, the addition of blebbistatin resulted in the expression of these 14 genes returning to basal levels, comparable to a flat control, further supporting the role of stress fiber formation and contractility in neuronal differentiation. Interestingly, Tuj1, an early neuronal differentiation marker, was not affected by the addition of blebbistatin or ML-7.

The role of nuclear deformation and associated protein lamin A/C were also investigated in the context of flat versus nano-grating neuronal differentiation.[80] ESC cultured with retinoic acid and neuronal differentiation media (positive neurogenesis control) displayed an increase in lamin A/C. Likewise, both MSC and ESC seeded on nano-grating patterns in the absence of retinoic acid for induction of neuronal differentiation showed increases in lamin A/C expression, as compared to the unpatterned controls. The authors also investigated H3K9me1 in MSC as another metric of neurogenesis. Cells seeded on nano-grating showed higher H3K9me1 on days 1 and 4; further culture resulted in no difference between the flat and nano-grating substrates. Notably, this study did not include pharmacological agent addition to establishing whether increased H3K9me1 and lamin A/C levels are directly caused by differing nanotopography, and instead relied on the paper discussed in the previous paragraph to establish the importance of nano-grating in substrate topography-mediated neurogenesis.

One archetypal study seeded induced pluripotent stem cells (iPSC) on nano-grating and nano-pillar arrays with differing widths, spacings, and depths [Figure 4].[81] Greater nanopattern height (560 nm) resulted in decreased spreading and greater alignment compliance for nano-grating. Concurrently, greater nanopattern height, regardless of topographical shape, resulted in higher cytoplasmic YAP. When combining increased nanopattern height with decreased nanopattern spacing, iPSC exhibited decreased proliferation. In agreement with observations of enhanced alignment and decreased

proliferation, iPSC on deep nano-grating substrates had higher expression of neuroectodermal-related (PAX6, day 6) and neuronal-related (Tuj1, day 14) genes. Immunostaining data at day 21 showed that both nano-gratings and nano-pillars increase mature neuronal markers (Tau and MAP2). Interestingly, nano-gratings seem to decrease the proportion of glutamatergic neurons and increase GABAergic neurons; however, no mechanistic explanation was offered.

One group generated mutant Rho GTPases to better characterize the enzyme's role in transducing substrate stiffness to NSC.[84] Dominant-negative RhoA and Cdc42 mutations caused the cells to become less stiff and more inclined to undergo neurogenesis, even on stiffer substrates normally conducive to astrogenesis. Likewise, constitutively active RhoA and Cdc42 caused moderate cell stiffening and bias towards astrogenesis despite culture on softer substrates. The mutant RhoA and Cdc42 cells responded to various contractility-affecting pharmacological agents (e.g. Y-27632 and blebbistatin) as anticipated (i.e. decreasing contractility rescued neurogenesis on compliant substrates for constitutively active RhoA). Should pharmacological manipulation and substrate stiffness modification be unfeasible, future studies can instead rely on mutant GTPases to enable substrate-independent control over the stem cell differentiation.

Another group incorporated a temporal aspect to nanotopography-mediated neurogenesis.[82] iPSC were chemically induced to dopaminergic neural progenitor cells on nano-grating patterns before transfer onto either another nano-grating or nano-pillar substrate. Tuj1, FOXA2 (a midbrain dopaminergic neuron marker), and tyrosine hydroxylase (an indicator of functional dopaminergic neurons) were found to be upregulated on nano-grating and nano-pillar substrates compared to flat substrates. The authors also sought to determine which nanotopgraphy generated more mature, "complex" neuron morphology. Nano-gratings resulted in neurons with longer neurite outgrowths, while nano-pillars enabled greater branch terminals, branch points, and dendritic complexity. The electrophysiological analysis showed cells transferred to nano-pillars to have a higher number of cells capable of repetitive spontaneous synaptic activity, as compared to cells on nano-pillar or flat substrates. These results suggest that while nano-gratings are sufficient to prime iPSC for a dopaminergic neurogenic pathway, nano-pillars may enable more mature neuronal morphology and function.

In a departure from typical nanoarrays with well-defined patterns, one group used reactive-ion etching (RIE) to generate heterogeneous "nanoroughness" substrates on vitronectin-coated glass for hESC and hiPSC.[83] Immunostaining after short-term culture (48 hours) showed greatly increased vinculin (associated with mature focal adhesions), actin (stress fibers), and cytoplasmic YAP when cells were seeded onto nanorough surfaces (RMS roughness = 200 nm). Interestingly, cells on nanorough substrates exhibited greatly accelerated conversion from pluripotent-associated gene expression regimen (e.g., Oct3/4, TERT) to neuroectoderm gene expression (e.g., PAX6, NeuroD1), even when growth (proliferation) media was used. Additionally, cells cultured on nanorough substrates were more responsive to directed differentiation into motor neurons (determined by $Olig2^+$, $Tuj1^+$, and $HB9^+$ staining) compared to cells on smooth controls throughout a 24-day differentiation and maturation period. As a final demonstration, lysophosphatidic acid,

which facilitates stress fiber formation, significantly reduced substrate-based differences in YAP localization (i.e., most YAP localized in nucleus regardless of roughness), resulting in decreased $PAX6^+$ cell. Interestingly, Y-27632 and cytochalasin D both increased cytoplasmic YAP localization (anticipated to increase neurogenesis) but either had no effect or decreased the percent of $PAX6^+$ cells (i.e., similar percent of $PAX6^+$ cells with or without these pharmaceutical agents for given roughness). Additional understanding of the underlying complexities is needed to fully elucidate the molecular mechanisms regulating neurogenesis.

3.2.3 Nanoarray Facilitated Maintenance of Stem Cell Pluripotency—Much like any other cells, induced pluripotent stem cells (iPSC) and embryonic stem cells (ESC) are subject to the same mechanotransduction signals and pathways, as discussed previously. Due to considerable clinical potential and instability during *in vitro* culture, the recapitulation of directed differentiation and maintenance of pluripotency are the two most significant areas of active research.[85] Since directed differentiation was discussed in earlier sections (MSC and NSC), we will focus on the maintenance of pluripotency as this aspect is unique to this particular class of stem cells.

Traditionally, iPSC was cultured on mouse embryonic fibroblast (MEF) feeder culture, which helps to condition the cell culture vessel.[86] With expanding knowledge of basic cell biology, significant efforts have been directed towards transitioning away from xenogenic feeder cell culture to naturally derived ECM-supported culture (e.g., Matrigel® from heterogeneous mouse sarcomas) for clinical translation.[86] The next goal in this field is to enable iPSC cultured on substrates with wholly human-derived ECM proteins. Kim et al. cultured human BJ1 fibroblasts to harvest the ECM deposited on conventional culture vessels.[86] These resulting ECM-coated vessels were subjected to decellularization and crosslinking with genipin, now termed fibroblast-derived matrices (FDM). Two distinct trends became evident when human ESCs were cultured on FDM of varying degrees of crosslinking and stiffness. Less crosslinked/softer FDM enabled greater cell attachment and proliferation, whereas FDM with higher crosslinking/Young's modulus maintained a greater proportion of alkaline phosphatase-positive (early pluripotency marker) colonies. They concluded that an intermediate-crosslinked FDM created an optimal balance between attachment/proliferation and pluripotency maintenance. This functional iPSC assay is supported by qPCR data, which showed uncrosslinked FDM decreased expression of genes coding for Oct4, E-cadherin, and other iPSC-associated proteins and increased expression of genes coding for N-cadherin, vimentin, and other mesenchymal-associated proteins. In light of these results, the authors suggested that substrate stiffness may affect the ability of iPSC to undergo an epithelial-to-mesenchymal transition. Studies such as these may play a key role in developing commercialized cell therapy manufacturing and compliance plans, where cell line quality assurance is significantly more rigorous than in basic research and development. This development represents an exciting intermediate between *in vitro* MEF feeder culture and *in vivo* acellular ECM, benefiting from the greater reproducibility inherent to *in vitro* culture, as well as cheaper production and absence of contaminating feeder cells and human-derived proteins.

iPSC and ESC typically grow as colonies on Matrigel or MEF feeder cultures, which are necessary for the maintenance of pluripotency. [85] Mechanotransduction protein RhoA, which mediates cytoskeletal contractility, is integral to maintaining E-cadherin, a protein involved with cell-cell contact. Loss of E-cadherin can result in apoptosis, disrupted colony formation, and loss of pluripotency. Perturbations to RhoA signaling (e.g., TGF-β, which activates RhoA) can cause preferential differentiation (e.g., mesenchymal and endodermal lineages with TGF-β). This is in agreement with the observation that iPSC have lower stiffness and cytoskeletal organization than fibroblasts, chondrocytes, and mesenchymal stem cells. Furthermore, mESC cultured on varying polyacrylamide gels (0.6–8kPa) reveals that softer substrates enable greater expression of the pluripotency gene Oct4 for significantly more cell passages. Caution is advised when designing soft substrates since excessively soft substrates (e.g., 0.1 kPa in one demonstration) may result in decreased viability and proliferation due to an inability to form prerequisite cytoskeletal elements. Additionally, supplementing and withdrawing specific soluble cues may cause cells to display different behaviors in response to the same substrate. In one instance, the removal of FGF-2 and TGF-β from culture media seemed to ablate the iPSC ability to maintain pluripotency based on substrate stiffness[85]. In another demonstration, honeycomb-shaped nanopattern substrates enabled iPSC to maintain elevated Oct4 expression only in the absence of FGF-2. The addition of FGF-2 caused the opposite effect in this particular report, wherein Oct4 was decreased when cells were seeded on honeycomb nanotopography.

By applying these mechanotransduction principles, Gerardo et al. have facilitated the reprogramming of MSC back to iPSC.[87] Umbilical cord-derived MSC (UC-MSC) were seeded onto tissue culture plastic (GPa range) or polydimethylsiloxane (PDMS) (15 kPa or 1.5 kPa), due to clinical interest owing to ease of access, relative immaturity/stemness compared to adult stem cells, and less exposure to external mutagens. Cells on stiff substrates presented flatter morphologies, while soft substrates allowed cells to adopt more columnar morphologies with greater cell-cell interactions along the Z-axis. As anticipated, stiffer substrates induced more robust stress fiber formation, larger focal adhesions, higher nuclear mechanical strain, and lower nuclear circularity. When probing the chromatin structure, MSC seeded on softer substrates exhibited lower DAPI fluorescence and higher H4K16ac levels, both of which are correlated with open, euchromatin regions commonly seen in pluripotent cells. To reprogram UC-MSC, polycistronic lentiviruses encoding the four canonical Yamanaka factors were administered to cells on retronectin-coated tissue culture plastic before replating on the aforementioned TCP/PDMS substrates.[87] MSC on soft substrates generated more iPSC-like colonies (e.g., SSEA-4 and TRA-1-60 positive) with greater reprogramming efficiency than cohorts on stiff substrates. They postulated that increasing euchromatin regions permits greater binding of exogenous reprogramming factors to the target sites, thus accelerating the expression of endogenous pluripotency-maintenance genes. These results indicate that seeding MSC on soft substrates to induce an iPSC-like “relaxed” cytoskeletal and nuclear phenotype prime the cells to undergo accelerated reprogramming.

Since iPSC tend to grow as colonies rather than single cells with limited cell-cell contact, one group sought to characterize the behavior of entire colonies on the nanotopography.[88] Both polyimide (periodicity of 650 nm, major study focus) and PDMS (periodicity of 340,

650, and 1400 nm) were employed in this study using light interference lithography to generate nano-grates with high fidelity. Single-cell iPSC aligned along the nano-grates as expected. Interestingly, iPSC within a colony center did not elongate along the direction of the nano-gratings, despite the overall colony displaying alignment. Rather than individual cells aligning, the authors observed cell division planes to be aligned perpendicular to the nano-grating. These findings suggest that nanotopographical surface patterns control entire colony morphology by influencing mitotic behavior along the colony periphery. PDMS substrates with the periodicity of 650 and 1400 nm mirrored these findings, though cells and colonies on 340 nm substrates notably showed no morphological differences, as compared to flat controls. Additionally, colonies seeded on nano-grating patterns responded more rapidly to BMP4 as a differentiation morphogen (e.g., downregulation of pluripotency genes Oct4 and Nanog) than colonies on flat substrates. This differential behavior based on individual iPSC position within the colony is substantiated by examination of YAP localization. Cells in the interior of the colony showed YAP localization in the cytoplasm, whereas cells on the periphery showed nuclear YAP localization. The significance of this paper is two-fold: (1) documentation of different iPSC behavior based on spatial location within a colony, and (2) creates motivation for the examination of other cell types for differential behavior between inner and peripheral cells.

4. Demonstrated applications of nanoarrays for electrochemical biosensing

While many biosensor designs exist and are currently under active investigation and refinement, certain aspects are universal. At a fundamental level, biosensors must be able to (1) recognize and record biological phenomena and (2) transduce that event into an electrical signal for further data processing. Analyte recognition is especially significant with samples that undergo minimal processing (e.g., whole blood samples) and are prone to extraneous biomolecules that mask the signal from the intended analyte. Some of the most popular capture elements include antibodies, oligonucleotides, and enzymes, which are notable for their high sensitivity and selectivity.[89, 90] For prolonged cell culture directly on the sensor, various ECM proteins and cell adhesion moieties may also be considered as capture elements that enable the sensor to interact with cells during culture. Certain applications involving sustained biological phenomena, such as the monitoring of stem cell differentiation over the course of several weeks, or materials that are scarce or costly to obtain, such as primary, freshly extracted cells from non-human primates, may benefit from the ability to read multiple data points from a single sample. Signal transduction is heavily dependent on what detection system is used. The three major detection systems currently in use are (1) optical, (2) physical, and (3) electrochemical.[89] Optical and electrochemical systems predominate the field for non-destructive, live-cell monitoring. Transduction systems may be relatively simple, as in H_2O_2 redox activity measurement on conductive substrates, or complex and involve biological systems, for instance, the cellular detection of biological analytes and secreted electrochemically-active molecules.[29, 31, 89–95]

Most popular and developed optical systems can be divided into four major subcategories: colorimetric, fluorescent, luminescent, and Raman scattering.[96] Colorimetric transduction

systems are the simplest sensing strategy, wherein a colored reagent can be observed by the naked eye, leading to rapid detection without complicated instruments. These are most limited by the imprecise nature and poor sensitivity of organoleptic detection. Fluorescence-based systems are the most common optical detection variant. A certain wavelength of light is used to excite the fluorophore to emit photons of a different wavelength, which are then detected. Advantages include high sensitivity, efficiency, and ease of use; disadvantages are primarily related to the specialized equipment, including monochromic light and filters used to separate excitation light from emitted light. Luminescence-based systems emit light without a prerequisite excitation light, resulting in a higher signal-to-noise ratio but still require equipment capable of converting photons into an electrical signal for accurate quantification. Raman scattering-based systems generally rely on surface-enhanced Raman scattering (SERS) to obtain an adequate signal for detection.[97] Apart from the requirement to tailor substrates specifically for SERS, potentially limiting micro- and nanotopopgrahy to influence cell behavior, special Raman microscopes must be employed to utilize this technique. Global limitations for optical biosensors include naturally turbid and complex biofluids which may contain optically absorbing and auto-fluorescing biomolecules.[98]

Here, we will focus on electrochemical detection using sensors with some form of micro- or nano-topography. Significant achievements in microelectronic circuit production make these sensors more readily available and translatable for clinical use, eliminating the need for specialized equipment, apart from the sensor itself.[98] Additionally, electrical signals from these sensors do not require additional transduction equipment for conversion of photons from optical biosensors into electrons via a charged-coupled device [CCD] cameras to produce a machine-readable signal, which increases performance.[98] Sensitivities as low as nanomolar concentrations are regularly reported with high selectivity against common biological contaminants, as detailed below. Many biological phenomena of interest, including expression of differentiation markers and key transcription factors, occur at very low concentrations, leading to this review's emphasis on electrochemical detection.

4.1 Roles of Nanomaterials in Electrochemical Biosensing

A variety of electrochemical sensing modalities have been developed, each with advantages and disadvantages.[21, 99] Controlled design of nanomaterials of different shapes, sizes, arrangements, and compositions can enhance these benefits and compensate for deficiencies, such as a weak signal-to-noise ratio. The exact nature of sensor-nanomaterial/topography interactions varies on a case-by-case basis, though some key concepts are reasonably consistent regardless of sensor type and target application. Electrochemical detection typically occurs at the sensor interface, which significantly increases with the property of nanomaterial (nonparallel surface-area-to-volume) and micro-/nanotopography.[89, 98] The increased surface area in turn typically translates to a higher measurement sensitivity due to (1) greater proportion of sensor mass affected by the target biological phenomena and (2) greater capture efficiency as a result of more enzymes present on a greater surface area that can capture a greater number of analyte molecules.[89, 98] Nanomaterials may impart additional functionalities to biosensors, such as enabling cell attachment, enhanced stability against fouling biological molecules, providing additional functional groups for chemical modifications, and improving electrical conductivity.[98] In many cases, metal-based

nanomaterials themselves may directly participate in chemical reactions as catalytic sites.[89, 98] Micro/nanotopographical features can be designed to enable interesting sensor architectures such as 3D porous hydrogel sensors with a dramatically increased surface area, as compared to flat 2D substrates, and enhanced spatial resolution when monitoring different areas of a sensor.[100, 101] Intelligent incorporation of nanomaterials and micro/nanotopography can significantly increase the utility of biosensors by improving performance and permitting additional functionalities. To this end, commonly used biocompatible nanomaterials will be categorized herein, and their uses in biosensors will be described. Key topics for this section will include unique physicochemical features, associated characterization techniques, and limitations for biological applications.[89, 90, 102]

4.1.1 Inorganic Metal (Oxide)—Metal nanomaterials have long been used in electrochemical sensing systems, owing to their excellent electrical conductivity, ease of synthesis, and surface modification potential with good biocompatibility.[103, 104] Decoration with metal nanomaterials can enhance the reactivity of the electrode by increasing the active surface area.[105] For example, Hsu et al. developed hemispherical pattern arrays on a silicon wafer by photolithography and sputtered Au nanoparticles.[106] The active sensing area was increased 10.2 times compared to the planar Au electrode, resulting in an improved detection limit of glucose (9 mM) and high sensitivity (749.2 $\mu A/cm^2 mM^1$). The oxidative current was stably maintained even after 20 potential cycles. Additionally, metals such as Au, Pt, and Ni and metal oxides such as Fe_3O_4, TiO_2, and NiO are also widely used in electrochemical biosensors as catalysts, which enable nonenzymatic detection of metabolites such as glucose and reactive oxygen species.[107–111] In particular, owing to the variety of the composites (e.g., Ni, NiO, $Ni(OH)_2$, etc.), nickel was most intensively examined transition metal for use as a catalyst.[107] In the case of glucose sensing, the redox couple of Ni^{2+}/Ni^{3+} is considered to be the reaction center of glucose oxidation, based on the coincidence of the anodic peak between the transition metal and glucose oxidation. Catalytic surfaces with $Ni(OH)_2$ (Ni^{2+}) are formed by the glucose oxidation process, followed by the oxidation of $Ni(OH)_2$ (Ni^{2+}) to NiOOH (Ni^{3+}) at a given potential. The oxidation of glucose molecules to gluconolactone can be realized by NiOOH (Ni^{3+}), which also enables the recycling of the $Ni(OH)_2$ (Ni^{2+}) for glucose oxidation. When glucose is applied to an Ni electrode, the anodic peak current rises, while the cathodic peak current remains the same. Furthermore, metal and metal oxide nanomaterials can directly promote conjugation to bio/chemical molecules based on intrinsic surface properties. For example, noble metals are known for their strong bonds with sulfur-containing molecules, and metal oxides are known to bind with carboxyl groups. In addition, as catalytic oxidation efficiency is highly affected by the surface state of metals and metal oxides, most of the oxidation processes are conducted in alkaline solutions. Though this unusual condition can enhance catalytic/sensing performance, it is not practical for real, biological sample analyses.

4.1.2 Conducting Polymers—Many kinds of conducting polymers such as polyaniline (PANI), poly(3,4-ethylene dioxythiophene) (PEDOT), and polypyrrole (PPy) are also considered as promising alternative materials for advanced electrochemical biosensors.[89, 92, 112–116] The advantages of conducting polymers mainly include the ease of synthesis, a relatively high electronic/ionic conductivity, and the capability to form highly uniform

arrays. The electrical conductivity of conducting polymers can be easily modulated by the doping degree. For example, when nonconductive polyaniline (PANI) is exposed to protonic acids such as HCl or camphor sulfonic acid, the nitrogen atoms on the imine group of the PANI backbone are protonated, where the pH-dependent degree of protonation results from its oxidation status.[92] Through the complete protonation of the emeraldine base form, conductivity can be increased by up to 10 orders of magnitude by forming a delocalized polysemiquinone radical cation. Though this mechanism is reversible through manipulation of the environmental conditions, these polymers can be utilized as transducers and can monitor pH through electrical conductivity changes. Interestingly, in this case, many electrons along the polymer backbone did not change during the doping process; however, the energy levels of polymers were rearranged. Conversely, other conducting polymers such as PEDOT and PPy can be doped through a redox reaction.[89] As these polymers are also nonconductive at normal conditions and possess a positively charged monomer unit on its backbone, they are prone to attract negatively charged dopants, which results in charge balancing on the polymer backbone with improved electrical conduction. Additionally, conducting polymers with well-defined redox behavior can function as good electrode materials for electrochemical sensing systems. However, their poor mechanical stability in aqueous electrolyte solutions restrains further progress in real applications during long-term cycling.

4.1.3 Carbon-based Materials—Carbon-based nanomaterials such as carbon nanotubes (CNTs), graphene, and its derivatives have been extensively studied and utilized for developing electrochemical sensing systems.[117–122] CNTs and pristine graphene are known to have similar conducting properties based on their unique structural arrangements.[123–125] The sp^2 carbon bond is perfectly arranged in a honeycomb lattice, which results in delocalization of π electrons across the planar plane. Carbon-based nanomaterials with oxygen-containing groups such as graphene derivates, including graphene oxide (GO) and reduced graphene oxide (rGO), are less conductive than the pristine carbon- based materials as the electron delocalization is disturbed by the formation of sp^3 carbon bonds. Thus, higher oxygen to carbon ratios result in a reduced electrical conductivity; however, this also known to be beneficial in some cases of the electrochemical sensing system. For example, oxygen-containing groups (e.g., carboxyl group) that are known as defects can promote the adhesion of primary amine-containing molecules or positively charged surfaces.[126] In addition, they can also serve as anchoring sites for metal nanoparticle formation for the development of nonenzymatic electrochemical sensing systems as well.[127, 128] Furthermore, doping with foreign atoms can also generate additional functionality for carbon-based materials.[123] For example, as nitrogen possesses five valence electrons and is similar in size to carbon, it is expected to form strong valence bonds with carbon atoms. Thus, nitrogen has been typically utilized for doping carbon-based materials, as the enhancement of conductivity could be expected based on the increased number of free charge carriers. In addition, nitrogen-doped carbon-based materials also exhibited excellent catalytic activity toward oxygen reduction reactions similar to metal nanoparticle decorations at certain conditions.[129] Furthermore, on carbon-based materials, a wide variety of aromatic group-containing bio/chemical molecules can noncovalently adsorb via strong $\pi-\pi$ interactions, which can preconcentrate the analytes on the electrode surface. However, these excellent

binding moieties provided by either pristine or oxidized carbon-based materials can promote surface fouling, which hampers the sensitivity and selectivity of electrochemical sensing systems as well.[126] Phenolic and amine compounds are particularly concerning, as they are universal in unprocessed biological samples.

4.2 Non-Destructive, Live-Cell Monitoring

One relatively simple study on non-destructive, live-cell monitoring was achieved by H_2O_2 monitoring. Shu et al. used MnO_2 nanosheets to cover a glass carbon electrode and electrochemically detected H_2O_2 [Figure 5].[91] The inclusion of the nanosheets resulted in a much greater reduction current under cyclic voltammetry, permitting amperometric detection of H_2O_2 concentrations as low as 5 μM with two linear ranges of 0.025–2 μM and 10–454 μM that were stable over at least 2 weeks and 100 scan cycles. The increased sensitivity was attributed to the catalytic reduction of H_2O_2 on the MnO_2 surface and porous nanostructure, leading to the high specific surface area. Moreover, the addition of uric acid, glucose, and ascorbic acid did not appreciably interfere with H_2O_2 amphoteric responses at −0.6V or subsequent H_2O_2 addition and detection. To examine the applicability of the sensor for the detection of H_2O_2 from live cells, Sp2/0 was cultured, suspended in PBS, and stimulated to release H_2O_2 via the addition of ascorbic acid. The detected signal was consistent with other reports (40 amol H_2O_2 per cell at 5 μM ascorbic acid for 10^7 cells in 4 mL PBS) and was not present in no cell, no ascorbic acid, and catalase controls. This study is a prototypical example of how nanomaterials can be used to improve the electrochemical detection of biologically relevant molecules. In order to improve electrochemical detection performance, electrochemical sensing systems have naturally led to designs incorporating multiple metal species. Zhu and coworkers focused on growing PtW nano-cubes on MoS_2 nanosheets via thermal decomposition.[31] The resulting hybrid nanocomposite was stable under ultrasonication and exhibited lower electron transfer resistance than the bare electrode surface or electrodes coated with MoS_2. Amperometric analysis at −0.25V showed detection to be linear from 1 μM to 200 μM, with a detection limit of 5 nM H_2O_2. Interestingly, Pt on MoS_2, PtW on graphene, and PtW on WS_2 all showed nonspecific responses to ascorbic acid and uric acid, whereas the PtW/MoS_2 system showed negligible disruption and enhanced specificity. Further specificity tests using dopamine, NO_3^-, K^+, 4-acetamidophenol, and hemoglobin showed the PtW/MoS_2 sensor to be unaffected and still capable of detecting further addition of H_2O_2. A cellular demonstration was conducted using 4T1 induced to release H_2O_2 via N-formyl methionyl leucyl phenylalanine (fMLP) stimulation. For this particular system, 2×10^6 cells could be induced to release a maximum of 25 nM H_2O_2 after stimulation with 2.2 μM fMLP, which is in agreement with other reports. As further work is done to enhance sensor specificity and sensitivity, more work investigating hybrid systems will become more commonplace. Similarly, Hu et al. deposited platinum nanoparticles and graphene on a sacrificial 3D porous nickel foam.[100] The resulting Pt/graphene scaffold enabled significantly higher specific surface area, which facilitated the charge/mass-transfer rate, overall conductivity, and A375 cell adhesion on the interior and exterior surfaces, as compared to a 2D Pt/graphene nanosheet counterpart. Interestingly, the 3D graphene foam was found to have a more positive Zeta potential than 2D graphene nanosheets. Reduced electrostatic repulsion between superoxide anions and 3D graphene foams, as compared to 2D nanosheets was proposed as a reason why 3D foams displayed better electrochemical

detection performance. Detection of superoxide anions (at 0.6μM) was found to be unimpeded by ascorbic acid, K^+, Na^+, Ca^{2+}, Cl^-, or NO_3^- up to 6.5 μM. When A375 cells were induced to release superoxide anions via zymosan, 3D Pt/graphene foams again showed greater sensitivity than 2D nanosheet films seeded with an equivalent number of cells. This demonstration shows that not only can 3D environments support better cell function but can also assist with electrochemical performance.

Although various electrochemical sensing systems have been extensively developed for monitoring soluble cell signaling components, it can be advantageous to develop a sensor that augments not only electrochemical detection but also enables direct monitoring of long-term live-cell growth. To this end, one group used WS_2 nanoflowers to coat carbon fiber electrochemical sensors for simultaneous H_2O_2 monitoring and cell culture.[29] The WS_2 nanosheets naturally adopted a flower-like structure after chemical vapor deposition, which dramatically increased specific surface area and exposed edge sites. An amperometric detection limit of 2 nM H_2O_2 was reported, which was not affected by the presence of superoxide anions or hypochlorite anions at a constant −0.25V. To demonstrate the *in vitro* applications of this sensor system, RAW 264.7 macrophages, and primary rat hippocampal neurons were cultured and induced to release H_2O_2 via N-formyl methionyl leucyl phenylalanine (fMLP) and epidermal growth factor (EGF), respectively. The authors demonstrated the detection of H_2O_2 from 0.3 μM fMLP and 500 ng/ml EGF from the respective test cells. Moreover, the EGF-induced signal can be attenuated by the addition of PD153035 (EGF receptor kinase domain inhibitor), wortmannin (phosphatidylinositol-3-OH kinase inhibitor), NSC23766 (NO synthase inhibitor), and apocynin (Nox inhibitor). This paper demonstrates not only an improvement to the field of metal- facilitated electrochemical detection (direct cell culture on sensors), it broadens the potential applications of such sensors to probing various cell-drug interactions so long as H_2O_2 is involved at some point in the interaction. In a more advanced manner, one communication of note from Lee et al. simultaneously investigated nanotopography to increase the efficacy of mesenchymal stem cell differentiation while enabling more sensitive electrochemical detection of key differentiation markers.[28] Arrays of graphene-coated gold nano-domes were fabricated with varying widths and pitch sizes, which served to modulate mechanotransduction signaling for osteogenesis. Dome widths of 400 nm were found to be the most conducive to osteogenesis, as measured by alkaline phosphatase [ALP] and osteocalcin expression. To demonstrate the platform for nondestructive stem cell differentiation monitoring, the authors used voltammetry for live cell, *in situ* ALP assays. The graphene-coated nano-domes enabled higher sensitivity towards the electrochemically active ALP reaction product, due to a higher electron transfer rate. Moreover, this system was used to nondestructively monitor osteogenesis over 3 weeks with corresponding increases in ALP electrochemical activity as culture time increased. This demonstrates the potential for the utilization of nanotopopgrahy and nanomaterials for multiple purposes, including the enhancement of stem cell differentiation and nondestructive monitoring [Figure 6a–c].

Furthermore, while many biosensors are serviceable *in vitro*, many researchers are trying to integrate conventional electrodes based on glass and metals into living animals but the methods are complicated by severe mechanical mismatch. To develop biosensors capable of

both *in vitro* and future *in vivo* sensing, Kireev et al. fabricated relatively flexible and soft polyimide substrates to detect cardiomyocyte electrophysiological function.[101] Since action potential-based ion movement was of interest, the authors utilized electrical impedance spectroscopy to monitor cardiomyocyte function. The fabricated sensors could be crumpled and would still function to record electrical activity from HL-1 cardiomyocytes. Cells were found to be able to proliferate on the sensor and generate action potential waveforms that are similar to those found elsewhere in the literature. Different electrode channels recorded signals with a time delay, indicating that action potentials propagate through the cell monolayer with potential future applications in spatially monitoring where and how action potentials behave throughout a tissue. Dissected rat embryonic heart tissue was placed on the flexible sensor and found to have a signal-to-noise ratio of approximately 50. Moreover, the shape of recorded action potentials shows typical P, Q, R, S, and T regions of normal electrocardiograms [Figure 6d–g]. For *in vivo* biosensing to become more clinically relevant, additional efforts, such as those described here, will be needed to address tissue-substrate mechanical mismatch.

5. Concluding Remarks and Future Perspectives

In this review, we summarized the recent advancements of nanoarray for stem cell-based therapy. The combination of extracellular environment modulation and precise stem cell behavior and function monitoring is the focus of functional nanoarrays. Through the review, we believe the ideal stem cell nanoarray should offer these distinct advantages: (1) biocompatibility, (2) nanotopographical cues capable of directing stem cell behaviors, and (3) enhanced sensitivity and selectivity to characterize cell fate and function non-destructively. In turn, the next-generation nanoarrays for cell monitoring and differentiation must leverage additional benefits from nanochemistry and material science. To this end, an increasingly interdisciplinary knowledge base is required to integrate these fields for the successful development of a clinically relevant product. Thus, advanced approaches are needed to utilize functional nanoarray for manipulating and monitoring stem cell behavior in realtime, which will lead to the development of materials and methods for treating numerous diseases and disorders.

Looking forward, key perspectives on both fabrication and biological analysis should be achieved. One of the primary barriers to nanotopography applications is the limited active surface area generated by the current fabrication techniques. Considering the real therapeutic approaches, clinical usage is still restricted, due to the limited size. Thus, developing a controllable and cost-effective nanoarray synthesis method that can be easily scaled up is one urgent requirement. Additionally, biocompatible flexible substrates can further facilitate clinical translation as well. Furthermore, understanding how the spatial structural morphology of nanoarrays contributes to different aspects, including the interfacial properties that affect the interaction with cells and electrical/electrochemical performances such as electron transfer rate, should be considered. A three-dimensional culture environment is also an aspect for which more information on the stem cell-environment regulation is required to understand the resulting cell signaling and epigenetic interactions.

This review also showcased how functional nanomaterials could provide answers to challenges in the field of biological analysis when applied as transducers for electrical/electrochemical biosensors. Ideal biosensors need to detect low abundance analytes from a small volume of the original matrix in a rapid, accurate, and inexpensive manner while maintaining long-term stability under the complex physiological assay environment. The successful integration of nanomaterials for cell-based biological analysis approaches must maintain function under physiological conditions such as high ionic strength and body temperatures. While these challenges can be overcome with proper surface modifications, a balance needs to be achieved between proper surface chemistry and the desired functionality in biosensing under physiological conditions.

Furthermore, there is still much room to improve beyond the nanoelectrode-based approaches for stem cell-based therapy. For example, it should be possible to perform stimulation and monitoring of stem cell differentiation simultaneously. Instead of direct electrical stimulation, nanoelectrode arrays can also be used for the highly topical, cell-specific delivery system for cell-controlling molecules, such as proteins, DNA, and nanoparticles, while altering integrin and cadherin ligations through topographical effects as well. To this end, we envision that the application of nanoarray in studies related to stem cell behavior and function will not only facilitate the implementation of stem cell therapies to treat degenerative diseases and injuries and but also drive stem cell therapy closer to clinical applications. This will ultimately lead to the development of methods, tools, drugs, and materials for treating numerous diseases and disorders. Thus, incorporating recent high-throughput screening approaches will likely be instrumental in the discovery of new drugs and materials and the design and development of novel materials to control and monitor stem cell fate.

Acknowledgments

J.-W.C. acknowledges partial financial support from the NRF (2019R1A2C3002300) and (2016R1A6A1A03012845) funded by MSIP and the ME of Korea. K.-B.L. acknowledges partial financial support from the NIH R21 (R21AR071101), NIH R01 (1R01DC016612, 3R01DC016612-01S1, and 5R01DC016612-02S1), New Jersey Commission on Spinal Cord Research (CSCR17IRG010 and CSCR16ERG019), and NSF (CBET-1803517). J.-H.L acknowledges partial financial support from the NRF (2019R1I1A1A01058779).

Notes and references

1. Ascherio A and Schwarzschild MA, Lancet Neurol, 2016, 15, 1257–1272. [PubMed: 27751556]
2. Trounson A and DeWitt ND, Nat Rev Mol Cell Biol, 2016, 17, 194–200. [PubMed: 26908143]
3. Fox IJ, Daley GQ, Goldman SA, Huard J, Kamp TJ and Trucco M, Science, 2014, 345, 1247391.
4. Knoepfler PS, Adv Drug Deliv Rev, 2015, 82–83, 192–196.
5. Sterneckert JL, Reinhardt P and Scholer HR, Nat Rev Genet, 2014, 15, 625–639. [PubMed: 25069490]
6. Dimmeler S, Ding S, Rando TA and Trounson A, Nat Med, 2014, 20, 814–821. [PubMed: 25100527]
7. Chen KG, Mallon BS, McKay RD and Robey PG, Cell Stem Cell, 2014, 14, 13–26. [PubMed: 24388173]
8. Shi Y, Inoue H, Wu JC and Yamanaka S, Nat Rev Drug Discov, 2017, 16, 115–130. [PubMed: 27980341]

9. Dalby MJ, Gadegaard N and Oreffo RO, Nat Mater, 2014, 13, 558–569. [PubMed: 24845995]
10. Wang X, Li S, Yan C, Liu P and Ding J, Nano Lett, 2015, 15, 1457–1467. [PubMed: 25697623]
11. Tsui JH, Janebodin K, Ieronimakis N, Yama DMP, Yang HS, Chavanachat R, Hays AL, Lee H, Reyes M and Kim DH, ACS Nano, 2017, 11, 11954–11968. [PubMed: 29156133]
12. Yang J, McNamara LE, Gadegaard N, Alakpa EV, Burgess KV, Meek RM and Dalby MJ, ACS Nano, 2014, 8, 9941–9953. [PubMed: 25227207]
13. Vining KH and Mooney DJ, Nat Rev Mol Cell Biol, 2017, 18, 728–742. [PubMed: 29115301]
14. Engler AJ, Sen S, Sweeney HL and Discher DE, Cell, 2006, 126, 677–689. [PubMed: 16923388]
15. Du J, Chen X, Liang X, Zhang G, Xu J, He L, Zhan Q, Feng XQ, Chien S and Yang C, Proc Natl Acad Sci U S A, 2011, 108, 9466–9471. [PubMed: 21593411]
16. Lv H, Li L, Sun M, Zhang Y, Chen L, Rong Y and Li Y, Stem Cell Res Ther, 2015, 6, 103. [PubMed: 26012510]
17. Brunner M, Mandier N, Gautier T, Chevalier G, Ribba AS, Guardiola P, Block MR and Bouvard D, PLoS One, 2018, 13, e0196021.
18. Shih YR, Tseng KF, Lai HY, Lin CH and Lee OK, J Bone Miner Res, 2011, 26, 730–738. [PubMed: 20939067]
19. Kegelman CD, Mason DE, Dawahare JH, Horan DJ, Vigil GD, Howard SS, Robling AG, Bellido TM and Boerckel JD, FASEB J, 2018, 32, 2706–2721. [PubMed: 29401582]
20. Wong KF, Liu AM, Hong W, Xu Z and Luk JM, Oncotarget, 2016, 7, 77683–77695. [PubMed: 27765911]
21. Wang PY, Thissen H and Kingshott P, Acta Biomater, 2016, 45, 31–59. [PubMed: 27596488]
22. Ngandu Mpoyi E, Cantini M, Reynolds PM, Gadegaard N, Dalby MJ and Salmerón-Sánchez M, ACS nano, 2016, 10, 6638–6647. [PubMed: 27391047]
23. Salmeron-Sanchez M and Dalby MJ, Chem Commun (Camb), 2016, 52, 13327–13336. [PubMed: 27722261]
24. Uhler C and Shivashankar GV, Nat Rev Mol Cell Biol, 2017, 18, 717–727. [PubMed: 29044247]
25. Nemati S, Kim SJ, Shin YM and Shin H, Nano Converg, 2019, 6, 36. [PubMed: 31701255]
26. Goodwin HS, Bicknese AR, Chien SN, Bogucki BD, Quinn CO and Wall DA, Biol Blood Marrow Transplant, 2001, 7, 581–588. [PubMed: 11760145]
27. Kim TH, Yea CH, Chueng ST, Yin PT, Conley B, Dardir K, Pak Y, Jung GY, Choi JW and Lee KB, Adv Mater, 2015, 27, 6356–6362. [PubMed: 26390254]
28. Lee JH, Choi HK, Yang L, Chueng SD, Choi JW and Lee KB, Adv Mater, 2018, 30, e1802762.
29. Tang J, Quan Y, Zhang Y, Jiang M, Al-Enizi AM, Kong B, An T, Wang W, Xia L and Gong X, Nanoscale, 2016, 8, 5786–5792. [PubMed: 26909564]
30. Lee JH, Choi JH, Chueng SD, Pongkulapa T, Yang L, Cho HY, Choi JW and Lee KB, ACS Nano, 2019, 13, 8793–8803. [PubMed: 31361458]
31. Zhu L, Zhang Y, Xu P, Wen W, Li X and Xu J, Biosens Bioelectron, 2016, 80, 601–606. [PubMed: 26897262]
32. Nguyen PK, Rhee JW and Wu JC, JAMA Cardiol, 2016, 1, 831–841. [PubMed: 27557438]
33. Mead B, Logan A, Berry M, Leadbeater W and Scheven BA, Stem Cells, 2017, 35, 61–67. [PubMed: 27273755]
34. Xue C, Shi X, Fang X, Tao H, Zhu H, Yu F, Ding X, Liu M, Fang F, Yang F, Wei Z, Chen T, Wang Z, Wang G, Cheng X, Wei J, Lin Y, Deng K, Wang X and Xin H, ACS Appl Mater Interfaces, 2016, 8, 8393–8400. [PubMed: 26974545]
35. Luo L, Jiang QP, Qin GH, Zhao K, Du GF, Wang H and Zhao HY, Sensors and Actuators B-Chemical, 2015, 218, 205–214.
36. Zhang M, Wang S, Li ZL, Liu CW, Miao R, He G, Zhao M, Xue J, Xia ZY, Wang YQ, Sun ZQ and Lv JG, Rsc Advances, 2019, 9, 3479–3485.
37. Zhao K, Du GF, Luo L, Qin GH, Jiang QP, Liu YJ and Zhao HY, Crystengcomm, 2015, 17, 2030–2040.
38. Zhou Y, Xi SQ, Yang XG and Wu HJ, Journal of Solid State Chemistry, 2019, 270, 398–406.

39. Gao F, Qin GH, Li YH, Jiang QP, Luo L, Zhao K, Liu YJ and Zhao HY, Rsc Advances, 2016, 6, 10298–10310.
40. Cook B, Liu QF, Liu JW, Gong MG, Ewing D, Casper M, Stramel A and Wu JD, Journal of Materials Chemistry C, 2017, 5, 10087–10093.
41. Wang SB, Wu YC, Miao R, Zhang MW, Lu XX, Zhang B, Kinstler A, Ren ZY, Guo YB, Lu TF, Suib SL and Gao PX, Crystengcomm, 2017, 19, 5128–5136.
42. Young C, Wang J, Kim J, Sugahara Y, Henzie J and Yamauchi Y, Chemistry of Materials, 2018, 30, 3379–3386.
43. Kang L, Zhang S, Li Q and Zhang J, J Am Chem Soc, 2016, 138, 6727–6730. [PubMed: 27177360]
44. Zhang X, Zhang Y, Yu BB, Yin XL, Jiang WJ, Jiang Y, Hu JS and Wan LJ, Journal of Materials Chemistry A, 2015, 3, 19277–19281.
45. Soci C, Zhang A, Xiang B, Dayeh SA, Aplin DP, Park J, Bao XY, Lo YH and Wang D, Nano Lett, 2007, 7, 1003–1009. [PubMed: 17358092]
46. Xu L, Li X, Zhan Z, Wang L, Feng S, Chai X, Lu W, Shen J, Weng Z and Sun J, ACS Appl Mater Interfaces, 2015, 7, 20264–20271. [PubMed: 26308593]
47. Chen Y, Zhang X and Xie Z, ACS Nano, 2015, 9, 8054–8063. [PubMed: 26259167]
48. Zhou H, Zou XP and Zhang YR, Electrochimica Acta, 2016, 192, 259–267.
49. Yu M, Ma YX, Liu JH and Li SM, Carbon, 2015, 87, 98–105.
50. Dong J, Ren L, Zhang Y, Cui X, Hu P and Xu J, Talanta, 2015, 132, 719–726. [PubMed: 25476370]
51. Tsyntsaru N, Silkin S, Cesiulis H, Guerrero M, Pellicer E and Sort J, Electrochimica Acta, 2016, 188, 589–601.
52. Wang X, Ye K, Zhang HY, Ma XK, Zhu K, Cheng K, Wang GL and Cao DX, International Journal of Hydrogen Energy, 2017, 42, 15044–15053.
53. Gioia D and Casella IG, Sensors and Actuators B: Chemical, 2016, 237, 400–407.
54. Martin CR, Science, 1994, 266, 1961–1966. [PubMed: 17836514]
55. Zhao C, Zhu Y, Chen L, Zhou S, Su Y, Ji X, Chen A, Gui X, Tang Z and Liu Z, Nanoscale, 2018, 10, 16278–16283. [PubMed: 30128448]
56. Ma XK, Ye K, Wang G, Duan MY, Cheng K, Wang GL and Cao DX, Applied Surface Science, 2017, 414, 353–360.
57. Xu Y, Zhou M, Wen LY, Wang CL, Zhao HP, Mi Y, Liang LY, Fu Q, Wu MH and Lei Y, Chemistry of Materials, 2015, 27, 4274–4280.
58. Guan XF, Chen D, Quan ZY, Jiang FX, Deng CH, Gehring GA and Xu XH, Nanoscale Res Lett, 2015, 10, 2419. [PubMed: 26055471]
59. Hao Q, Huang H, Fan X, Hou X, Yin Y, Li W, Si L, Nan H, Wang H, Mei Y, Qiu T and Chu PK, Nanotechnology, 2017, 28, 105301.
60. Robatjazi H, Bahauddin SM, Macfarlan LH, Fu SD and Thomann I, Chemistry of Materials, 2016, 28, 4546–4553.
61. Wen L, Xu R, Mi Y and Lei Y, Nat Nanotechnol, 2017, 12, 244–250. [PubMed: 27893732]
62. Wen L, Xu R, Cui C, Tang W, Mi Y, Lu X, Zeng Z, Suib SL, Gao PX and Lei Y, Nano Lett, 2018, 18, 4914–4921. [PubMed: 29986140]
63. Abagnale G, Steger M, Nguyen VH, Hersch N, Sechi A, Joussen S, Denecke B, Merkel R, Hoffmann B, Dreser A, Schnakenberg U, Gillner A and Wagner W, Biomaterials, 2015, 61, 316–326. [PubMed: 26026844]
64. Yang C, Tibbitt MW, Basta L and Anseth KS, Nat Mater, 2014, 13, 645–652. [PubMed: 24633344]
65. Bornes TD, Jomha NM, Mulet-Sierra A and Adesida AB, Tissue Eng Part C-Me, 2016, 22, 208–220.
66. Hunziker EB, Quinn TM and Hauselmann HJ, Osteoarthritis Cartilage, 2002, 10, 564–572. [PubMed: 12127837]
67. Moghadasi Boroujeni S, Mashayekhan S, Vakilian S, Ardeshirylajimi A and Soleimani M, J Biomed Mater Res A, 2016, 104, 1610–1621. [PubMed: 26879731]

68. Li R, Xu J, Wong DSH, Li J, Zhao P and Bian L, Biomaterials, 2017, 145, 33–43. [PubMed: 28843065]
69. Lee MS and Yang HS, Biotechnol J, 2017, 12, 1700309.
70. Carson D, Hnilova M, Yang X, Nemeth CL, Tsui JH, Smith AS, Jiao A, Regnier M, Murry CE, Tamerler C and Kim DH, ACS Appl Mater Interfaces, 2016, 8, 21923–21932. [PubMed: 26866596]
71. Jiang T, Kai D, Liu S, Huang X, Heng S, Zhao J, Chan BQY, Loh XJ, Zhu Y, Mao C and Zheng L, Biomaterials, 2018, 178, 281–292. [PubMed: 29945065]
72. Wu Y, Yang Z, Law JB, He AY, Abbas AA, Denslin V, Kamarul T, Hui JH and Lee EH, Tissue Eng Part A, 2017, 23, 43–54. [PubMed: 27824280]
73. Zhao C, Wang X, Gao L, Jing L, Zhou Q and Chang J, Acta Biomater, 2018, 73, 509–521. [PubMed: 29678674]
74. Qian W, Gong L, Cui X, Zhang Z, Bajpai A, Liu C, Castillo AB, Teo JCM and Chen W, ACS Appl Mater Interfaces, 2017, 9, 41794–41806. [PubMed: 29116745]
75. Assoian RK, Bade ND, Cameron CV and Stebe KJ, Open Biol, 2019, 9, 190155.
76. Sophia Fox AJ, Bedi A and Rodeo SA, Sports Health, 2009, 1, 461–468. [PubMed: 23015907]
77. Leipzig ND and Shoichet MS, Biomaterials, 2009, 30, 6867–6878. [PubMed: 19775749]
78. Shah S, Yin PT, Uehara TM, Chueng ST, Yang L and Lee KB, Adv Mater, 2014, 26, 3673–3680. [PubMed: 24668911]
79. Ankam S, Lim CK and Yim EK, Biomaterials, 2015, 47, 20–28. [PubMed: 25682157]
80. Ankam S, Teo BKK, Pohan G, Ho SWL, Lim CK and Yim EKF, Front Bioeng Biotechnol, 2018, 6, 69. [PubMed: 29904629]
81. Song L, Wang K, Li Y and Yang Y, Colloids Surf B Biointerfaces, 2016, 148, 49–58. [PubMed: 27591570]
82. Tan KKB, Lim WWM, Chai C, Kukumberg M, Lim KL, Goh ELK and Yim EKF, Sci Rep, 2018, 8, 9567. [PubMed: 29934644]
83. Chen W, Han S, Qian W, Weng S, Yang H, Sun Y, Villa-Diaz LG, Krebsbach PH and Fu J, Nanoscale, 2018, 10, 3556–3565. [PubMed: 29410983]
84. Keung AJ, de Juan-Pardo EM, Schaffer DV and Kumar S, Stem Cells, 2011, 29, 1886–1897. [PubMed: 21956892]
85. Ireland RG and Simmons CA, Stem Cells, 2015, 33, 3187–3196. [PubMed: 26189759]
86. Kim IG, Gil CH, Seo J, Park SJ, Subbiah R, Jung TH, Kim JS, Jeong YH, Chung HM, Lee JH, Lee MR, Moon SH and Park K, Biomaterials, 2018, 150, 100–111. [PubMed: 29035736]
87. Gerardo H, Lima A, Carvalho J, Ramos JRD, Couceiro S, Travasso RDM, Pires das Neves R and Graos M, Sci Rep, 2019, 9, 9086. [PubMed: 31235788]
88. Abagnale G, Sechi A, Steger M, Zhou Q, Kuo CC, Aydin G, Schalla C, Muller-Newen G, Zenke M, Costa IG, van Rijn P, Gillner A and Wagner W, Stem Cell Reports, 2017, 9, 654–666. [PubMed: 28757164]
89. Shavanova K, Bakakina Y, Burkova I, Shtepliuk I, Viter R, Ubelis A, Beni V, Starodub N, Yakimova R and Khranovskyy V, Sensors (Basel), 2016, 16, 223. [PubMed: 26861346]
90. Moon JM, Thapliyal N, Hussain KK, Goyal RN and Shim YB, Biosens Bioelectron, 2018, 102, 540–552. [PubMed: 29220802]
91. Shu Y, Xu J, Chen JY, Xu Q, Xiao X, Jin DQ, Pang H and Hu XY, Sensors and Actuators B-Chemical, 2017, 252, 72–78.
92. Li L, Wang Y, Pan L, Shi Y, Cheng W, Shi Y and Yu G, Nano Lett, 2015, 15, 1146–1151. [PubMed: 25569673]
93. Hempel F, Law JK, Nguyen TC, Munief W, Lu X, Pachauri V, Susloparova A, Vu XT and Ingebrandt S, Biosens Bioelectron, 2017, 93, 132–138. [PubMed: 27666366]
94. Liu H, Weng L and Yang C, Microchimica Acta, 2017, 184, 1267–1283.
95. Nam B, Ko T-K, Hyun S-K and Lee C, Nano Convergence, 2019, 6, 40. [PubMed: 31832881]
96. Majdinasab M, Mitsubayashi K and Marty JL, Trends Biotechnol, 2019, 37, 898–915. [PubMed: 30777309]

97. El-Said WA, Kim T-H, Kim H and Choi J-W, PloS one, 2011, 6.
98. Grieshaber D, MacKenzie R, Voros J and Reimhult E, Sensors (Basel), 2008, 8, 1400–1458. [PubMed: 27879772]
99. El-Said WA, Yoon J and Choi JW, Nano Converg, 2018, 5, 11. [PubMed: 29721403]
100. Hu FX, Guo CX, Yang HB, Shi ZZ, Wang M, Xue YH, Zhu L, Chen T, Dai LM and Li CM, Sensors and Actuators B-Chemical, 2019, 287, 209–217.
101. Kireev D, Seyock S, Ernst M, Maybeck V, Wolfrum B and Offenhausser A, Biosensors (Basel), 2016, 7, 1.
102. Guo D, Lai LF, Cao AM, Liu HK, Dou SX and Ma JM, Rsc Advances, 2015, 5, 55856–55869.
103. Wang Y, Shan X, Wang H, Wang S and Tao N, J Am Chem Soc, 2017, 139, 1376–1379. [PubMed: 28088852]
104. Yusoff N, Pandikumar A, Ramaraj R, Lim HN and Huang NM, Microchimica Acta, 2015, 182, 2091–2114.
105. Vilian ATE, Kim W, Park B, Oh SY, Kim T, Huh YS, Hwangbo CK and Han YK, Biosens Bioelectron, 2019, 142, 111549.
106. Hsu CW, Su FC, Peng PY, Young HT, Liao S and Wang GJ, Sensors and Actuators B-Chemical, 2016, 230, 559–565.
107. Fleischmann M, Korinek K and Pletcher D, Journal of Electroanalytical Chemistry and Interfacial Electrochemistry, 1971, 31, 39–49.
108. Zhu H, Li L, Zhou W, Shao ZP and Chen XJ, Journal of Materials Chemistry B, 2016, 4, 7333–7349. [PubMed: 32263734]
109. Niu XH, Li X, Pan JM, He YF, Qiu FX and Yan YS, Rsc Advances, 2016, 6, 84893–84905.
110. Xie FY, Liu TT, Xie LS, Sun XP and Luo YL, Sensors and Actuators B-Chemical, 2018, 255, 2794–2799.
111. Tee SY, Teng CP and Ye E, Mater Sci Eng C Mater Biol Appl, 2017, 70, 1018–1030. [PubMed: 27772701]
112. Valiūnienė A, Rekertaitė AI, Ramanavičienė A, Mikoliūnaitė L and Ramanavičius A, Colloids and Surfaces A: Physicochemical and Engineering Aspects, 2017, 532, 165–171.
113. Jain R, Jadon N and Pawaiya A, Trac-Trends in Analytical Chemistry, 2017, 97, 363–373.
114. Xu G, Jarjes ZA, Desprez V, Kilmartin PA and Travas-Sejdic J, Biosens Bioelectron, 2018, 107, 184–191. [PubMed: 29459331]
115. Wang G, Han R, Su X, Li Y, Xu G and Luo X, Biosens Bioelectron, 2017, 92, 396–401. [PubMed: 27829555]
116. Chao Z, Govindaraju S, Giribabu K, Huh YS and Yun K, Sensors and Actuators B-Chemical, 2017, 252, 616–623.
117. Tan F, Cong LC, Li XN, Zhao Q, Zhao HX, Quan X and Chen JW, Sensors and Actuators B-Chemical, 2016, 233, 599–606.
118. Bollella P, Fusco G, Tortolini C, Sanzo G, Favero G, Gorton L and Antiochia R, Biosens Bioelectron, 2017, 89, 152–166. [PubMed: 27132999]
119. Lee H, Choi TK, Lee YB, Cho HR, Ghaffari R, Wang L, Choi HJ, Chung TD, Lu N, Hyeon T, Choi SH and Kim DH, Nat Nanotechnol, 2016, 11, 566–572. [PubMed: 26999482]
120. Bahadür EB and Sezgintürk MK, TrAC Trends in Analytical Chemistry, 2016, 76, 1–14.
121. Song Y, Luo Y, Zhu C, Li H, Du D and Lin Y, Biosens Bioelectron, 2016, 76, 195–212. [PubMed: 26187396]
122. Hondred JA, Breger JC, Alves NJ, Trammell SA, Walper SA, Medintz IL and Claussen JC, ACS Appl Mater Interfaces, 2018, 10, 11125–11134. [PubMed: 29504744]
123. Kim TH, Lee D and Choi JW, Biosens Bioelectron, 2017, 94, 485–499. [PubMed: 28342377]
124. Lee JH, Park SJ and Choi JW, Nanomaterials (Basel), 2019, 9, 297.
125. Pumera M, Materials Today, 2011, 14, 308–315.
126. Vicarelli L, Heerema SJ, Dekker C and Zandbergen HW, ACS Nano, 2015, 9, 3428–3435. [PubMed: 25864552]

127. Wei W, Wang G, Yang S, Feng X and Mullen K, J Am Chem Soc, 2015, 137, 5576–5581. [PubMed: 25849066]
128. Ju J and Chen W, Anal Chem, 2015, 87, 1903–1910. [PubMed: 25533846]
129. Tang Y, Allen BL, Kauffman DR and Star A, J Am Chem Soc, 2009, 131, 13200–13201. [PubMed: 19722487]

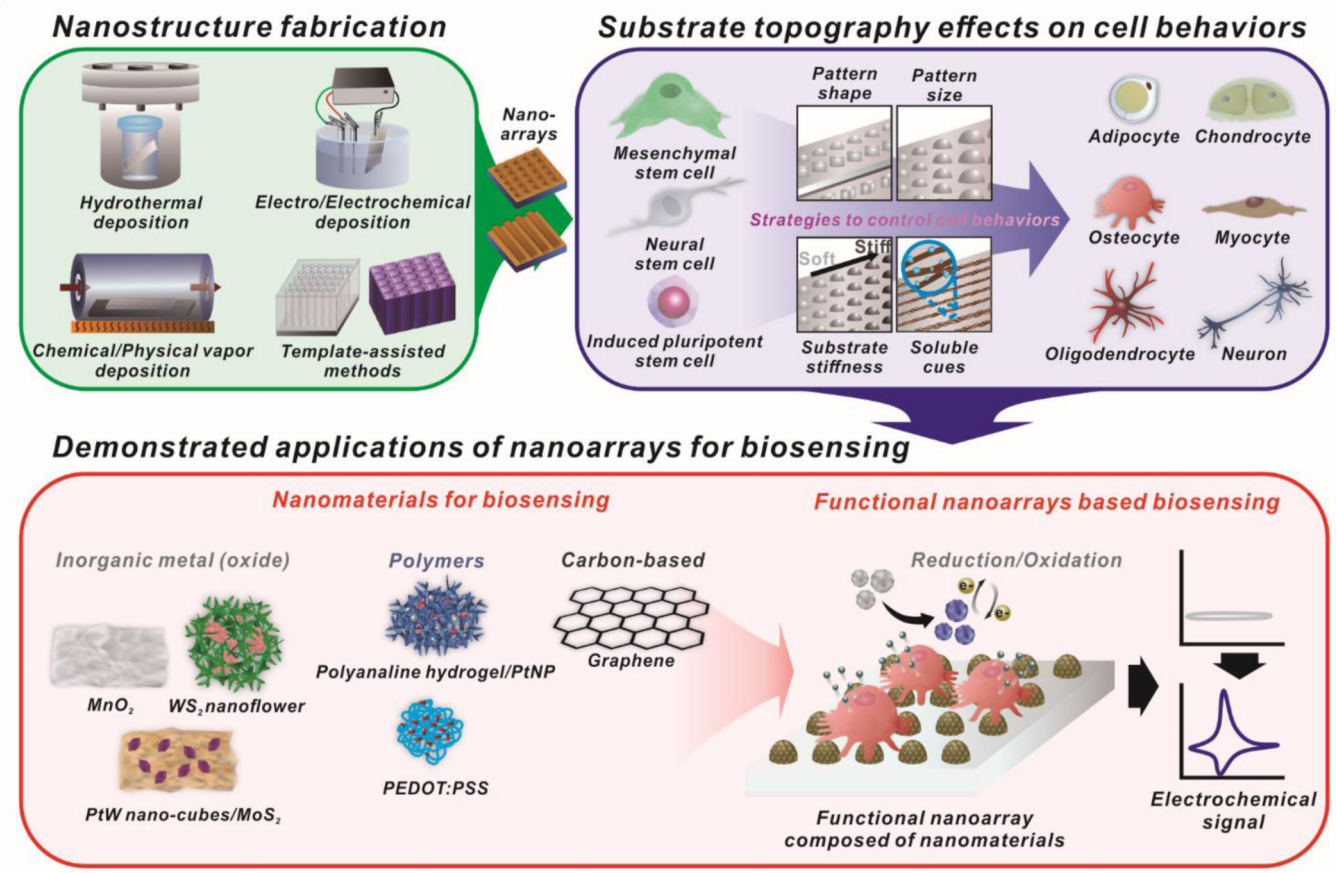

Figure. 1.

Schematic illustration of functional nanoarrays for investigating stem cell fate and functions.

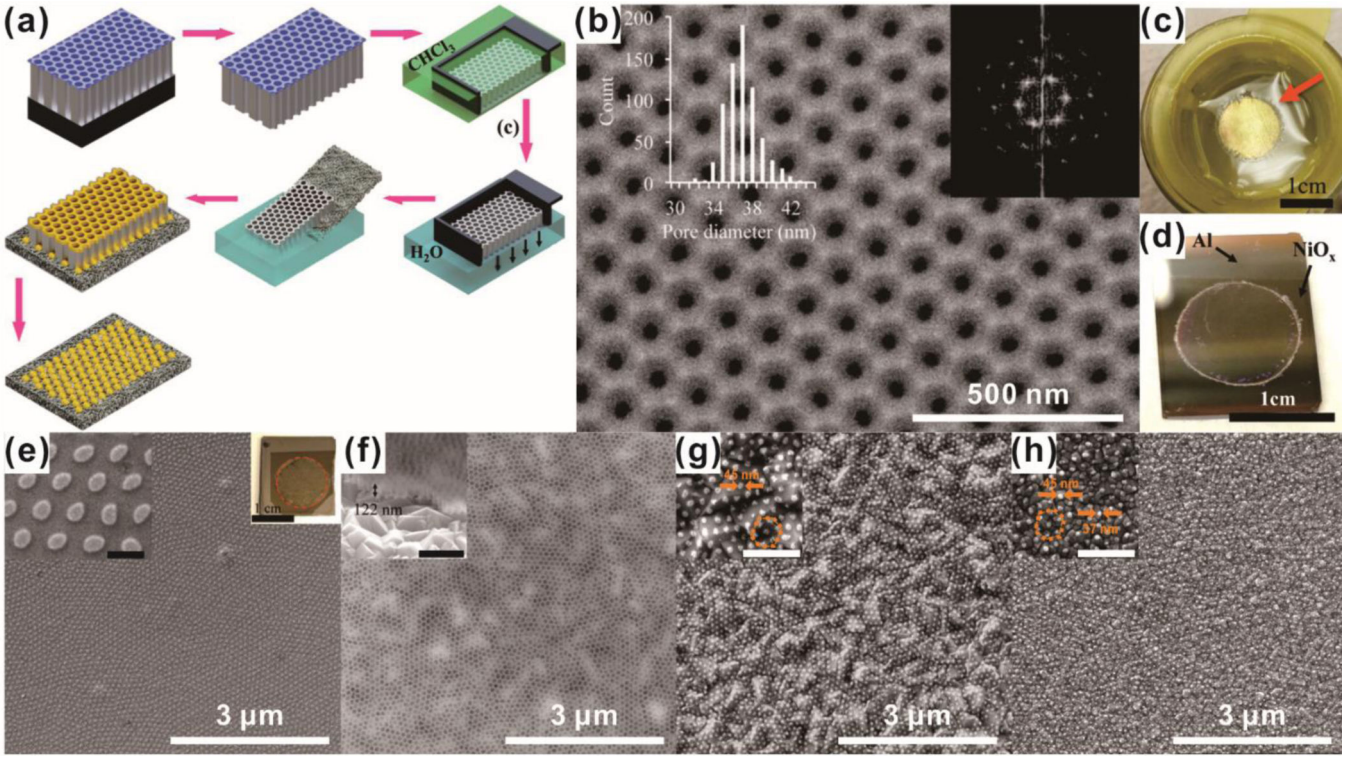

Figure. 2.

Fabrication of a nanodot array based on the template-assisted method. (a) Illustration of the fabrication process of an AAO pattern template using ultrathin alumina membranes (UTAM). (b) SEM image of the fabricated template. (c) Digital image of the fabricated template floating on water. (d) Transfer of the fabricated template. (e) SEM image of fabricated nickel nanodot arrays using a template. (f) Plain and oblique view an SEM image of transferred nanodot arrays. (g, h) Fabrication of gold nanodot arrays using a template-assisted method on an FTO substrate (g) and an ITO substrate (h). Scale bars in inset images of (e)-(h) are 500 nm. Reprinted with permission from ref. 60.

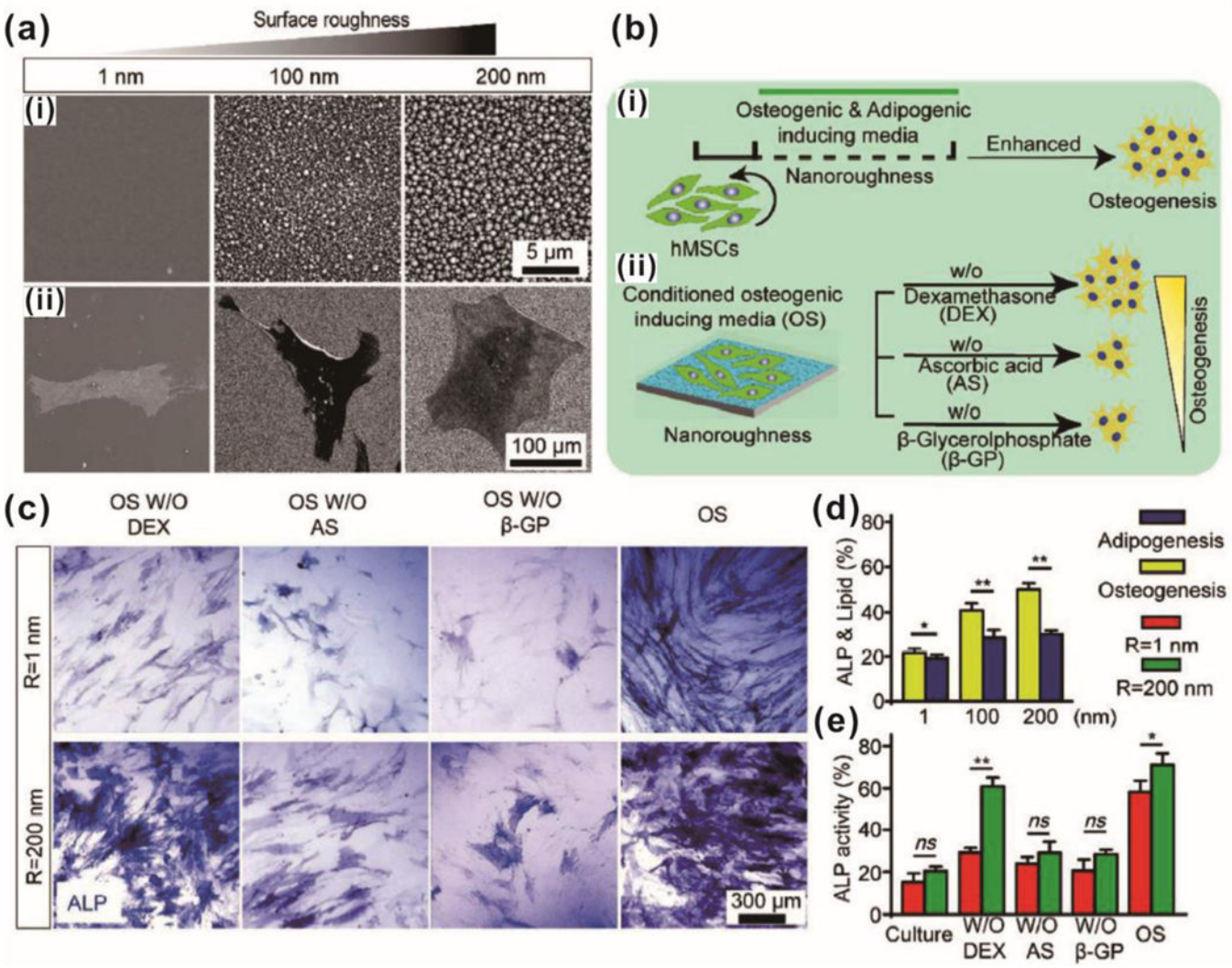

Figure. 3.

Enhanced osteogenic differentiation of MSC using a nanotopographic substrate. (a) SEM images of (i) nanotopographic substrate and (ii) cultured MSC on the substrate. (b) Schematic illustration of the experimental design for osteogenic differentiation of MSC using nanotopographic substrate. (c) ALP staining of osteogenic differentiated MSC on a smooth and nanorough substrate. (d) Quantifications of osteogenic and adipogenic differentiation of MSC on the nanotopographic substrate using ALP staining and oil-red lipid staining. (e) Quantification of osteogenic differentiation for MSC on the nanotopographic substrate in conditioned media. Reprinted with permission from ref. 74.

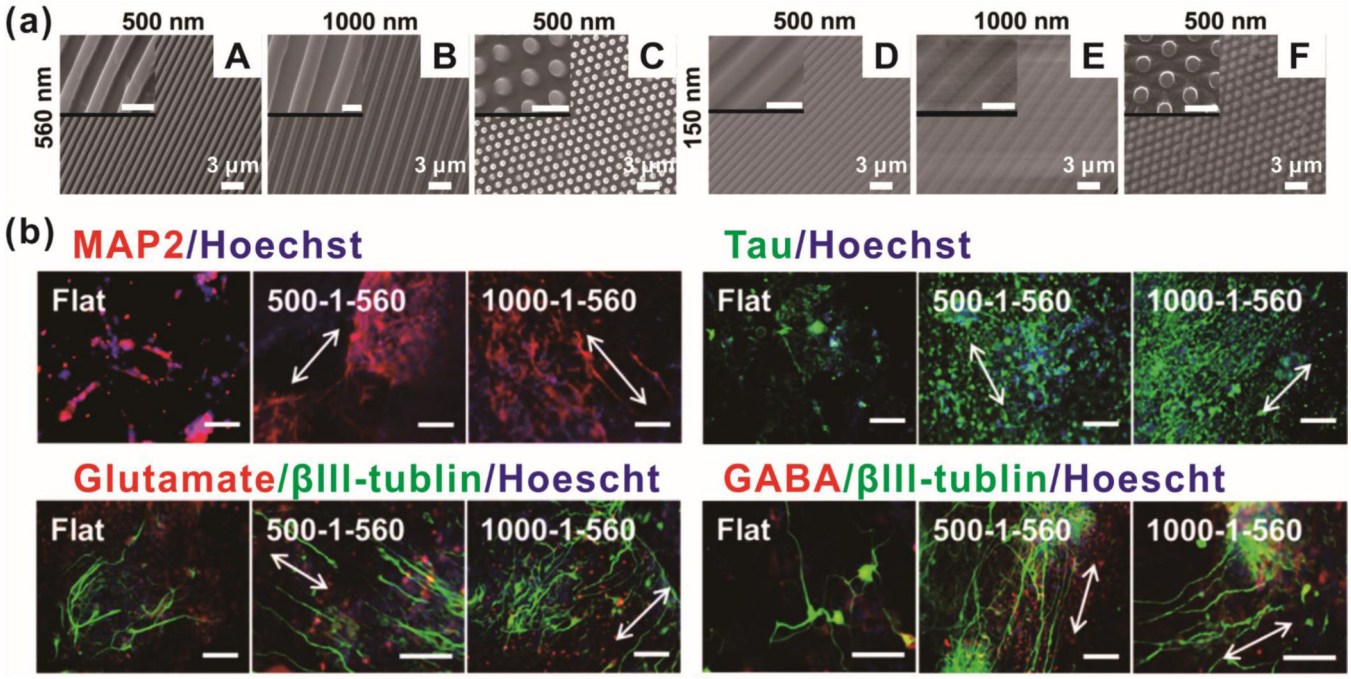

Figure. 4.

Neurogenesis of hiPSCs on nanoarrays (nanogratings and nanopillars). (a) SEM images of nanoarrays. Gap size and width size of nanogratings were synchronized as 500 nm (A, D) and 1000 nm (B, E). The diameter of the nanopillar was 500 nm, which was 1.9 times the diameter in center-to-center spacing (C, F). The heights of the nanoarrays were 560 nm (A, B, C) and 150 nm (D, E, F). Scale bars in inset images are 1 μm. (b) Expression of neuronal markers after differentiation on nanoarrays. Scale bars are 100 μm. Reprinted with permission from ref. 81.

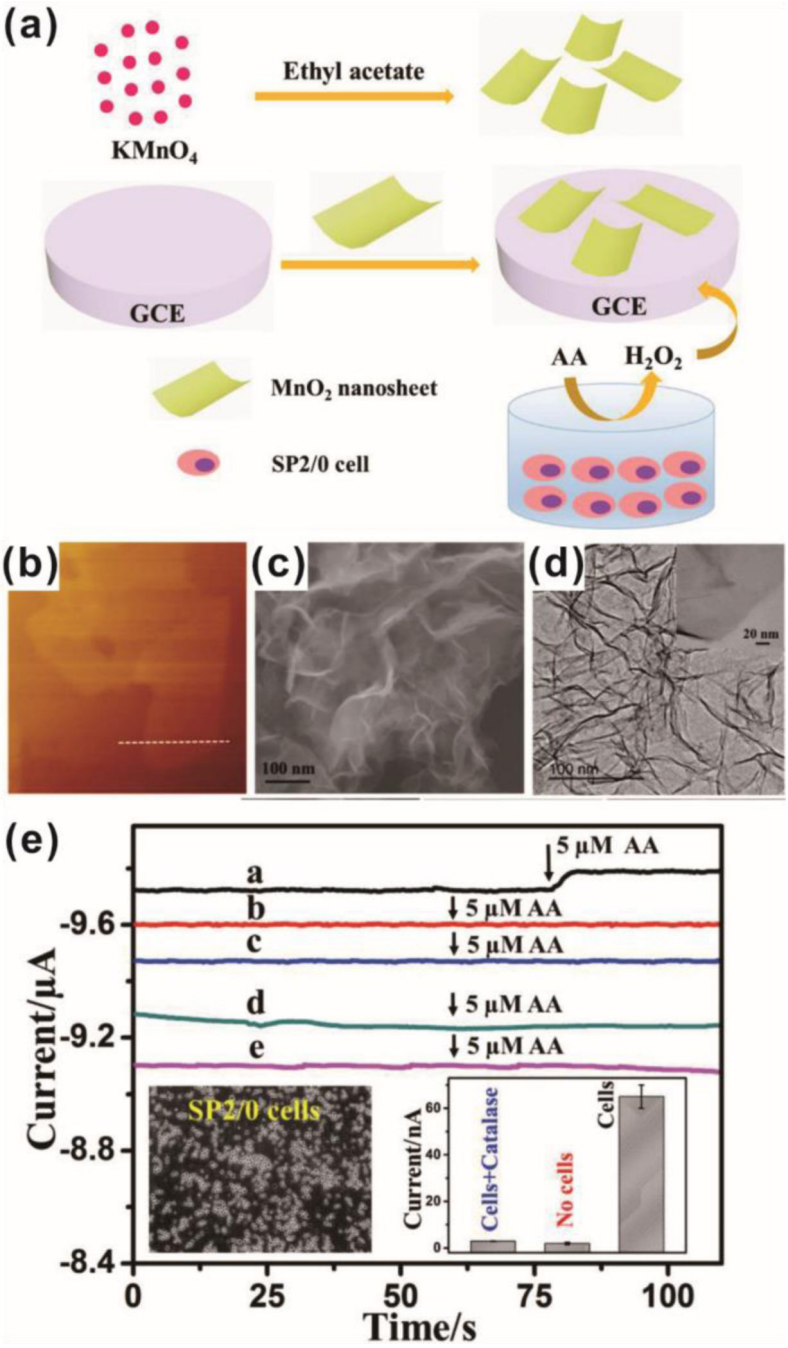

Figure. 5.

Non-destructive, live-cell monitoring technique by H_2O_2 monitoring using MnO_2 nanosheets on a glass carbon electrode (GCE). (a) Schematic illustration of H_2O_2 detection from SP2/0 cells. (b-d) Characterization of MnO_2 nanosheets. (e) Amperometric *i-t* curves of the response of GCE with MnO_2 nanosheets (curve a) and without MnO2 nanosheets (curve d) for the reduction of H_2O_2 released from SP2/0 cells. Amperometric *i-t* curves of the response of GCE with MnO_2 nanosheets (curve b) and without MnO_2 nanosheets (curve e) in the absence of SP2/0 cells. Amperometric *i-t* curves of the response of GCE with

MnO_2 nanosheets (curve c) in the presence of SP2/0 cells and catalase. Reprinted with permission from ref. 91.

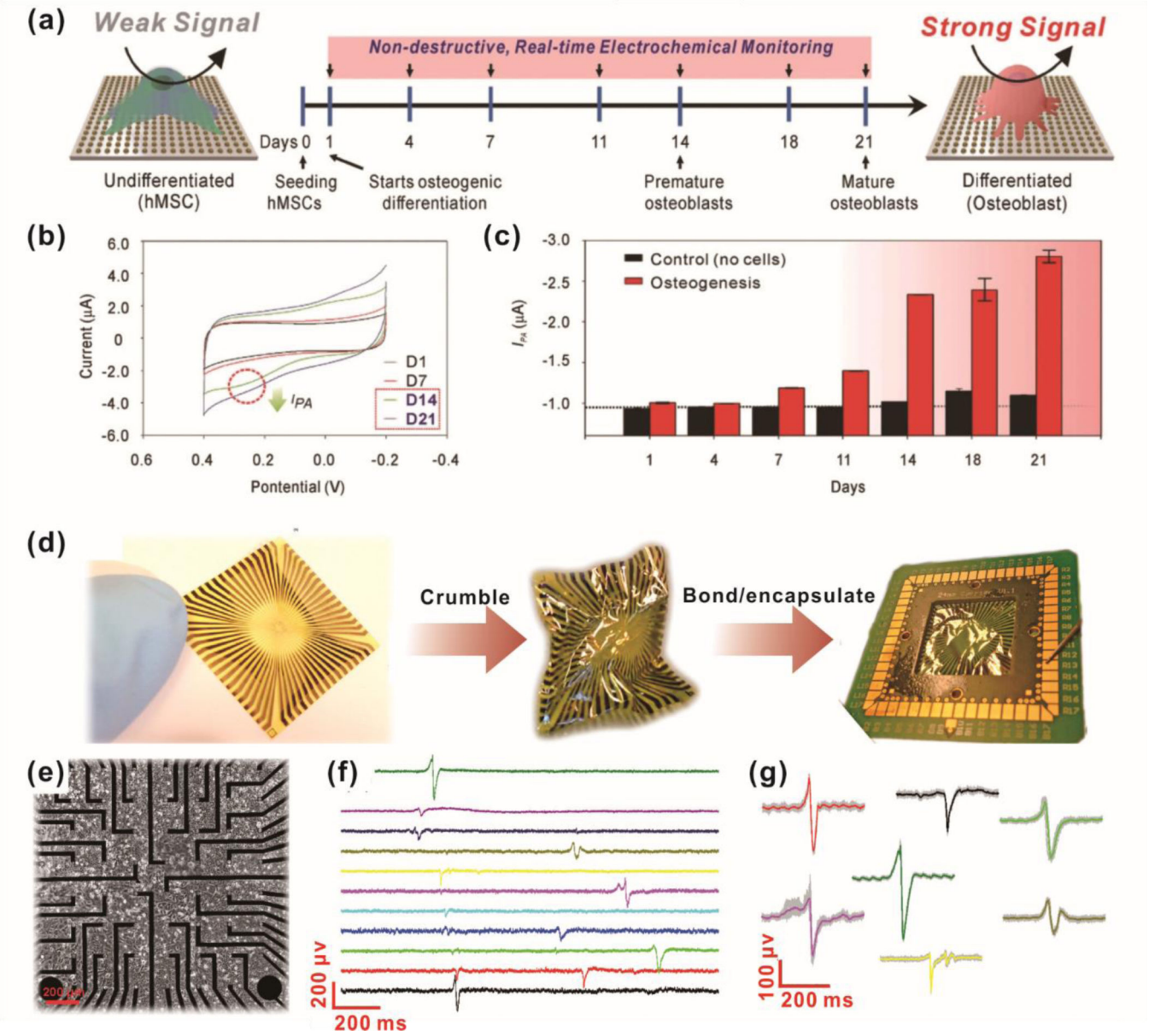

Figure. 6.

Non-destructive, live-cell monitoring methods using electrochemical sensing (a-e) and electrophysiological sensing (d-g). (a) Schematic diagram of electrochemical signal change during osteogenic differentiation of MSC on the nanoarray composed of gold and reduced graphene oxide. (b) Cyclic voltammogram of cultured MSC on the nanoarray from time-dependent monitoring (Day 0 to Day 21). (c) The cathodic peak currents of MSC cultured nanoarray from day 1 to day 21. (d) Tested graphene microelectrodes for heart tissue recording. A flexible chip was crumbled to mechanical deformation, then soldered and encapsulated. (e) Picture of HL-1 cells seeded on graphene microelectrodes. (f) Time trace recordings of HL-1 cells on 11 different channels of graphene microelectrodes. (g) The variety of recorded action potential shapes from different HL-1. (a)-(e) are reprinted with

permission from ref. 28. © 2018 WILEY-VCH Verlag GmbH & Co. KGaA, Weinheim, and (d)-(g) are reprinted with permission from ref. 101.

Table. 1

Mesenchymal stem cell differentiation with topography effects of nanoarray

Cell	Nanoarray	Differentiation	Ref.
MSC	PCL/PLLA nanofiber	Myogenesis	67
	Fibrillar hydrogel	Chondrogenesis	68
	Nanopatterned-PUA	Myogenesis	69
	PCL-PTHF	Chondrogenesis	71
	PCL/PLA/PGA nano-grating. nano-pillar	Chondrogenesis	72
	PI nano-patterns	Adipogenesis/Osteogenesis	63
	HA nanorod	Osteogenesis	73
	Nanorough	Osteogenesis	74

Table. 2

Neural stem cell differentiation with topography effects of nanoarray

Cell	Nanoarray	Differentiation	Ref.
NSC	Hydrogel	Oligodendrogenesis	77
	PCL nanofiber	Oligodendrogenesis	78
	Nano-grating	Neurogenesis	79
	Nano-grating	Neurogenesis	80
	Nano-grating/ nano-pillar	Neurogenesis	81
	Nanograte/ nanopillar	Neurogenesis	82
	Nanoroughness	Motor-neurogenesis	83

Table. 3

iPSC with topography effects of nanoarray

Cell	Nanoarray	Effect	Ref.
iPSC	Polyacrylamide gel	Pluripotency	85
	ECM coated vessel	Proliferation/Pluripotency	86
	PDMS	Pluripotency	87
	PI/PDMS nano-grates	Colony alignment	88

Table. 4

Nanomaterials for biosensing

Material		Target of detection	Ref.
Inorganic metal	Hemisphere Au	Glucose	106
	Pt-nanocube on MoS_2	H_2O_2	31
	MnO_2	H_2O_2	91
	WS_2	H_2O_2	29
Polymer	PANI	Uric acid Cholesterol Triglycerides	92
	Polyimide	Electrophysiological signal	101
Carbon-based	Pt/graphene nanosheet	Superoxide anion	100
	Graphene-Au	Alkaline phosphatase	28